N-Type Calcium Channel Inactivation Probed by Gating-Current Analysis

Lisa P. Jones, Carla D. DeMaria, and David T. Yue
Program in Molecular and Cellular Systems Physiology, Departments of Biomedical Engineering and Neuroscience, Johns Hopkins University School of Medicine, Baltimore, Maryland 21205 USA

ABSTRACT N-type calcium channels inactivate most rapidly in response to moderate, not extreme depolarization. This behavior reflects an inactivation rate that bears a U-shaped dependence on voltage. Despite this apparent similarity to calcium-dependent inactivation, N-type channel inactivation is insensitive to the identity of divalent charge carrier and, in some reports, to the level of internal buffering of divalent cations. Hence, the inactivation of N-type channels fits poorly with the "classic" profile for either voltage-dependent or calcium-dependent inactivation. To investigate this unusual inactivation behavior, we expressed recombinant N-type calcium channels in mammalian HEK 293 cells, permitting in-depth correlation of ionic current inactivation with potential alterations of gating current properties. Such correlative measurements have been particularly useful in distinguishing among various inactivation mechanisms in other voltage-gated channels. Our main results are the following: 1) The degree of gating charge immobilization was unchanged by the block of ionic current and precisely matched by the extent of ionic current inactivation. These results argue for a purely voltage-dependent mechanism of inactivation. 2) The inactivation rate was fastest at a voltage where only ~⅓ of the total gating charge had moved. This unusual experimental finding implies that inactivation occurs most rapidly from intermediate closed conformations along the activation pathway, as we demonstrate with novel analytic arguments applied to coupled-inactivation schemes. These results provide strong, complementary support for a "preferential closed-state" inactivation mechanism, recently proposed on the basis of ionic current measurements of recombinant N-type channels (Patil et al., 1998. *Neuron.* 20:1027–1038).

INTRODUCTION

Voltage-gated calcium channels provide a primary pathway for Ca^{2+} entry into neurons. As such, calcium channel inactivation could produce widely variable depression of Ca^{2+} influx according to the history of neuronal activity, with many potential functional implications, including enhanced short-term depression of synaptic efficacy (e.g., Borst et al., 1997; Forsythe et al., 1998). Despite the enormous physiological impact of such inactivation, the underlying mechanisms for neuronal calcium channels are still incompletely understood. Two "classic" mechanisms have been described (Hille, 1992). Like voltage-gated sodium and potassium channels, certain neuronal calcium channels (e.g., Zhang et al., 1994) inactivate by a voltage-dependent mechanism in which the intrinsic voltage dependence of certain gating transitions favors entry into inactivated states upon depolarization (Hodgkin and Huxley, 1952; Armstrong and Bezanilla, 1977). Characteristic hallmarks of conventional voltage-dependent inactivation include (Fox, 1981): 1) insensitivity of inactivation properties to the species of charge carrier and 2) monotonic acceleration of inactivation rate with increasing depolarization. Unlike sodium and potassium channels, some calcium channels exhibit an alternative, calcium-sensitive form of inactivation, in which the accumulation of intracellular calcium ions speeds inactivation to provide physiological feedback (Eckert and Chad, 1984). For example, calcium channels in *Aplysia* neurons (Brehm and Eckert, 1978) manifest the following distinctive properties of calcium inactivation: 1) the calcium-current magnitude (whether varied by voltage or by external ion concentration) largely specifies the speed of inactivation, resulting in a U-shaped dependence of inactivation rate on voltage; 2) the charge carrier species markedly affects the inactivation rate, with Ba^{2+} being much less effective than Ca^{2+}; and 3) increased intracellular buffering of divalent cations inhibits inactivation. These two "classic" mechanisms are not mutually exclusive, as snail neuron calcium channels may inactivate via both of these two forms of inactivation (Gutnick et al., 1989).

However, many neuronal calcium channels exhibit properties that square poorly with the archetypal profile for either of the "classic" mechanisms of inactivation. The incongruities are particularly apparent for N-type channels, which (along with P/Q-type channels) predominate in triggering neurotransmitter release (Dunlap et al., 1995). Both recombinant (Patil et al., 1998) and native (Kasai and Aosaki, 1988; Jones and Marks, 1989; Cox and Dunlap, 1994) N-type calcium channels demonstrate a deep, U-shaped dependence of inactivation rate upon voltage that is indistinguishable with Ba^{2+} or Ca^{2+} as charge carrier. Furthermore, N-type channel inactivation is weakly sensitive or completely insensitive to internal divalent cation buffering in some systems (Jones and Marks, 1989; Patil et al., 1998, respectively), although not in others (Kasai and Aosaki, 1988; Cox and Dunlap, 1994). These findings demonstrate that N-type channels inactivate by an unorthodox mechanism. Proposed explanations include variant schemes of calcium-sensitive inactivation in which Ba^{2+} and Ca^{2+} are equipotent at accelerating inactivation (Kasai and Aosaki,

Received for publication 9 July 1998 and in final form 10 February 1999.
Address reprint requests to Dr. David T. Yue, Department of Biomedical Engineering, The Johns Hopkins School of Medicine, 713 Ross Bldg., 720 Rutland Ave., Baltimore, MD 21209. Tel.: 410-955-0078; Fax: 410-955-0549; E-mail: dyue@bme.jhubme.jhu.edu.

0006-3495/99/05/2530/23 $2.00

1988; Cox and Dunlap, 1994), as well as differing, unconventional models of voltage-dependent inactivation (Jones and Marks, 1989; Patil et al., 1998).

Defining the interrelation between inactivation and gating currents arising from channel (de)activation could be critical to clarifying N-type channel inactivation, as has proved to be the case for understanding inactivation in voltage-gated sodium channels (Armstrong and Bezanilla, 1977; Bezanilla et al., 1982; Vandenberg and Bezanilla, 1991); potassium channels (Bezanilla et al., 1991; Fedida et al., 1996; Olcese et al., 1997; Roux et al., 1998); and cardiac, L-type (α_{1C}) calcium channels (Bean and Rios, 1989; Hadley and Lederer, 1991a, b; Shirokov et al., 1992, 1993; Ferreira et al., 1997). In particular, voltage-dependent inactivation of sodium, potassium, and L-type calcium channels partially "immobilizes" (Armstrong and Bezanilla, 1977) the movement of charge-bearing voltage sensors that underlie channel activation, thereby reducing measurable gating current. Such immobilization argues that voltage-dependent inactivation and channel activation are mechanistically coupled processes. In striking contrast, calcium-sensitive inactivation of L-type (α_{1C}) calcium channels, produced by short depolarizing pulses that minimize voltage-dependent inactivation, profoundly inhibits ionic current without affecting gating-charge movement (Hadley and Lederer, 1991b; Shirokov et al., 1993). This result implies that calcium-sensitive inactivation is largely independent of channel activation. Because voltage-dependent and calcium-sensitive mechanisms of inactivation have been distinguished by their contrasting effects on gating currents, correlative examination of gating currents and inactivation might be particularly useful in probing N-type calcium channel inactivation.

The coexistence of multiple species of voltage-gated channels in neurons has made it difficult to obtain such information about neuronal calcium channels. Hence we express recombinant N-type channels in mammalian HEK 293 cells to provide a homogeneous population of voltage-gated channels, thereby facilitating measurements of pure N-type channel gating current and its modulation by inactivation. These experiments offer the first glimpse of how inactivation of neuronal calcium channels affects the voltage sensor movement that supports channel activation. We find that the degree of gating charge immobilization bears a one-to-one correspondence to the extent of inactivation, fitting with a voltage-dependent mechanism of inactivation. The rate of inactivation is maximal at a voltage where only $\sim$⅓ of the gating charge has moved from its fully resting configuration. This unusual experimental result implies that inactivation occurs most rapidly from intermediate closed conformations along the activation pathway, as we demonstrate with analytic arguments applied to coupled activation schemes. These results provide strong, complementary support for a "preferential closed-state" inactivation mechanism, recently proposed on the basis of ionic current measurements of recombinant N-type channels (Patil et al., 1998).

MATERIALS AND METHODS

Expression of N-type channels

HEK 293 cells were transiently transfected with a total of 10 μg of α_{1B} (human $\alpha_{1B\text{-}1}$; Williams et al., 1992), 10 μg of the $\alpha_2\delta$ subunit (Tomlinson et al., 1993), and 10 μg of a β subunit (β_{1b}, Pragnell et al., 1991; β_{2a}, Perez-Reyes et al., 1992; or β_3, Castellano et al., 1993). Standard transfection and culture methods were employed, as previously described in Jones et al. (1998).

Electrophysiology

Whole-cell recordings were acquired, sampled, and filtered largely as described in Jones et al. (1998). Series resistance averaged 4 MΩ and was compensated by 75–85%. Average cell capacity was 17 pF. Voltage pulses were delivered every 30–45 s for inactivation protocols and every 15–20 s for activation protocols, from a holding potential (HP) of −100 mV. Leak and capacity currents were subtracted using a P/8 protocol for ionic currents, and either a P/-5 or a P/-8 protocol for gating currents, all delivered from −100 mV.

The base external solution contained (in mM) 155 *N*-methyl-D-glucamine (NMG) aspartate; 10 HEPES; 10 4-aminopyridine; 0.1 EGTA (pH 7.4 with NMG, 280–300 mOsm with no added charge carrier). The internal solution contained (in mM) 150 NMG-methanesulfonate ($MeSO_3$); 1 $MgCl_2$; 4 MgATP; 10 HEPES; 10 EGTA, 2 GDPβS (pH 7.3 with NMG, typically 280–290 mOsm). For experiments using 2 μM ω-conotoxin GVIA (ω-CTX) (Alamone Labs), 0.05% (w/v) fatty-acid-free bovine serum albumin (Sigma) was added to the external solution. External solution flowed continuously at a rate of 1–2 ml/min during recording.

Ionic currents were measured with 2 mM $CaCl_2$ added to the external solution. Calcium was chosen to reduce the surface charge shift between solutions used in ionic and gating current measurements (see Figs. 4 *A* and 5 *B*). To assay ionic current inactivation, a 100-ms depolarization to potentials ranging from −80 mV to 60 mV was followed by a test pulse to the peak of the current-voltage relation (typically −10 mV) to determine the fraction of noninactivated current. In most cases, before the prepulse, we included a 10-ms normalizing depolarization to −10 mV (see Fig. 2 *A*, *top*), which provided a normalizing current that could be used to factor out any slow drift in current levels. The degree of inactivation was calculated by normalizing test-pulse ionic currents by the test-pulse current after a hyperpolarizing prepulse to −80 mV, before averaging across cells. For channels containing β_3, where a prepulse to −80 mV produces significant inactivation, this method for normalization may result in an underestimate of the true degree of inactivation.

Activation curves for ionic current (*G-V* relations) were measured using 30-ms test depolarizations ranging from −80 to +60 mV. Subsequent repolarization was to −50 mV to allow good resolution of tail currents. For each cell, plots of peak tail current at −50 mV (I_{tail}) versus test-pulse voltage (V_{test}) were normalized by an estimate of maximum peak tail current ($I_{tail,max}$). $I_{tail,max}$ was taken as the saturating value of a Boltzmann fit to the I_{tail}-V_{test} data. The resulting normalized relations are equivalent to normalized P_o-V relations and are referred to as *G-V* curves. *G-V* curves were averaged across cells.

For gating currents, ionic currents were blocked by an external solution containing 0.2 mM $LaCl_3$/2 mM $MgCl_2$ (Jones et al., 1998). The effective free La^{3+} concentration was 0.1 mM because of the presence of 0.1 mM EGTA in all external solutions. Gating charge moved during a voltage jump was calculated as the integral over the epoch, taking as baseline the last 3 ms of the test pulse, and is referred to as Q_{on} or Q_{off} for depolarizing and hyperpolarizing voltage jumps, respectively. To test for effects of inactivation on gating-charge mobility, the voltage protocol was identical to that used for characterizing ionic-current inactivation, except that the test pulse was typically to +45 mV (Figs. 3 and 5) to allow measurement of Q_{max} (maximum amount of mobile charge). The normalizing test pulse was to +45 mV for β_3. The degree of gating charge immobilization was determined by normalizing the charge moved during the test pulse ($Q_{on,test}$) by the $Q_{on,test}$ after a prepulse to −80 mV, before averaging across cells.

The voltage dependence of charge movement (Q-V relations; Fig. 4) was measured using a protocol identical to that used for G-V relations, except that hyperpolarization was to −100 mV after the test pulse. For each cell, Q_{on}-V and Q_{off}-V curves were normalized by an estimate of maximum mobile charge (Q_{max}), taken as the saturating value of a Boltzmann fit to the Q_{on}-V. Such normalized Q_{on}-V and Q_{off}-V curves were averaged across cells.

In our leak subtraction protocol, leak pulses were delivered after a 400-ms repolarization to the holding potential (−100 mV) after the primary test stimulus. Therefore, we were concerned that inactivation produced by preceding test depolarizations might shift the voltage dependence of a component of gating charge movement (Bezanilla et al., 1982; Brum and Rios, 1987; Shirokov et al., 1992) into the range of our leak pulses. Several lines of evidence argue against this possibility. In a cell transfected with $\alpha_{1B\text{-}1}\,\beta_3\,\alpha_2\delta$ with $Q_{max} \approx 200$ fC, opposite polarity voltage jumps still sum to zero (Fig. 1 *A*), even after a 10-s prepulse to −60 mV to inactivate ionic current. In some cells, the cancellation was not quite as complete, but the apparent nonlinear charge movement over this voltage range (−90 to −150 mV) moved slowly ($\tau \sim 6$ ms) and amounted to <20% of immobilized charge. More to the point, any such nonlinear charge movement was undetectable in the specific leak-subtraction protocols (−100 to −130 mV) used in this study (Fig. 1 *B*), where the extent of immobilization does not depend on the leak subtraction protocol. At the top, we illustrate leak-subtracted test-pulse currents for a stimulus either without (*left*) or with (*middle*) a prepulse, in addition to the difference trace (*far right*), to illustrate the reduction in charge movement. Below we show the non-leak-subtracted data (*solid lines*) and the scaled leaks (*dashed lines*). Note that the difference in raw data traces (*a–c*, *solid trace*, *far right*) closely resembles the difference between leak-subtracted traces (*e–f*, *far right*), indicating that charge immobilization reflects a reduction in test pulse charge movement, as opposed to increased gating charge movement in the leak trace after a prepulse. Consistent with this idea, there is little difference between the leaks (*b–d*, *dashed trace*, *far right*), apart from a transient spike that is due to slow drift in the passive electrical properties of the patch. Confirmatory results (Fig. 1 *B*) were obtained in two other cells. This analysis indicates that the observed decrease in gating charge mobility

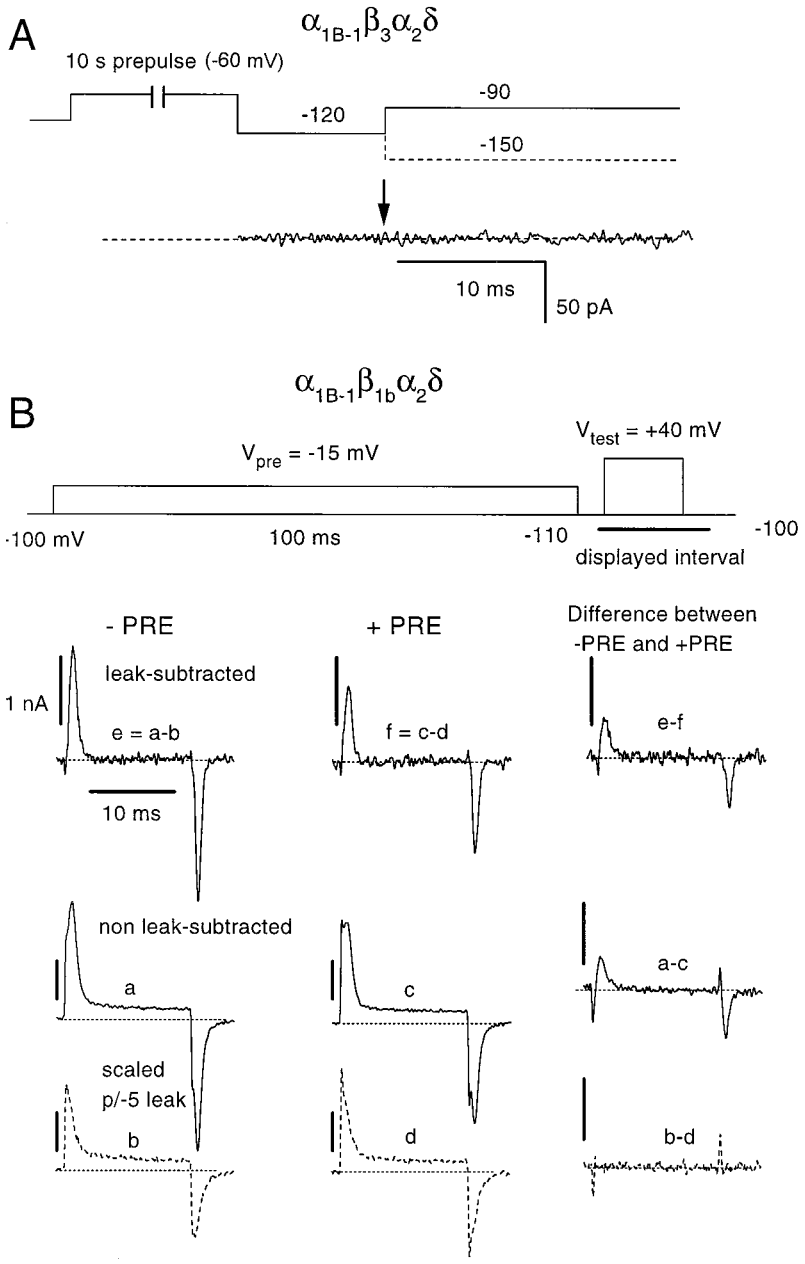

FIGURE 1 Leak subtraction control experiments. All displayed traces were recorded in 2 mM Mg^{2+}/0.2 mM La^{3+} block solution. (*A*) Membrane properties between −90 and −150 mV are linear, despite a prolonged 10-s prepulse to −60 mV. The sum of currents elicited by opposite polarity jumps (*top*, *solid and dashed lines*) is essentially zero, indicating that membrane properties are linear over the voltage range used for leak pulses, even in the presence of substantial inactivation. Data are from cell 378_8, transfected with $\alpha_{1B\text{-}1}\,\beta_3\,\alpha_2\delta$. (*B*) Gating currents with or without a 100-ms prepulse to −15 mV. (*Top row*) Leak-subtracted currents were taken from the "displayed region," which spans a test pulse to +40 mV. Test-pulse currents were elicited with (*top row*, *middle*) or without (*top row*, *left*) a prepulse. Subtraction of these two currents yields a nonzero difference trace (*top row*, *right*), which quantifies the apparent extent of gating charge immobilization. (*Middle and bottom rows*) Test pulse currents illustrating non-leak-subtracted data (*solid lines*, *middle row*) and scaled leak pulse currents (*dotted line*, P/-5, *bottom row*) used to calculate the leak-subtracted traces (*top*). The rightmost panel again displays the difference between test pulse currents with and without a prepulse. All vertical scale bars correspond to 0.1 nA. Data are from cell 312_9, transfected with $\alpha_{1B\text{-}1}\,\beta_{1b}\,\alpha_2\delta$.

is not due to contamination of leak traces by "charge 2" (Brum and Rios, 1987).

Data analysis

Fits in figures to either *G-V* or *Q-V* relations were performed with dual-Boltzmann functions of the form

$$f_{low}/(1 + \exp[-(z_{low}F/RT)(V - V_{1/2,low})]) + f_{high}/(1 + \exp[-(z_{high}F/RT)(V - V_{1/2,high})])$$

where f is the amplitude, z is the effective charge, and $V_{1/2}$ is the midpoint of activation of the low- and high-threshold components, with parameters adjusted by eye. Fits to prepulse-inactivation relations were also determined by eye, using arbitrary theoretical functions. All reported values are mean ± SEM.

RESULTS

Fig. 2 confirms that recombinant N-type ($\alpha_{1B\text{-}1}$ β_{1b} $\alpha_2\delta$) Ca^{2+} currents exhibit an unusual form of inactivation. The detailed prepulse inactivation protocol is shown at the top of Fig. 2 *A*. A brief pulse to −10 mV precedes the 100-ms prepulse, providing a normalizing current that allows us to monitor the stability of currents over time. The exemplar Ca^{2+} currents shown below (Fig. 2 *A*) serve to illustrate two characteristic features of N-type channel inactivation. First, appreciable prepulse inactivation is already apparent with prepulse voltages at (or below) the threshold of activation (Fig. 2 *A*, −40 mV trace), indicating that current-independent, closed-state inactivation is present. The normalizing pulse is not responsible for this inactivation, as essentially identical results are obtained using a prepulse protocol without such a pulse (data not shown). Second, the inactivation rate does not increase monotonically with voltage. Because steady-state inactivation is essentially complete at voltages greater than or equal to −40 mV (Patil et al., 1998, and below), we consider the marked U-shaped relation between test-pulse current and prepulse potential (for 100-ms prepulse durations) to be a measure of kinetic properties of inactivation (Fig. 2 *B*, *filled symbols*). Accordingly, the maximum rate of inactivation occurs at an intermediate potential (−20 mV, in this case) and thereafter decreases with increasing prepulse potential. The upturn of this I_{test}-V_{pre} relation with strong prepulse depolarization is not due to voltage-dependent relief of channel inhibition by G proteins (Patil et al., 1996), because G-protein inhibition was minimized by dialysis with 2 mM GDPβS (Ikeda, 1991; also see the Discussion). Nor is the upturn of the prepulse-inactivation curve obligatorily related to a decrease in Ca^{2+} entry as the prepulse voltage approaches the reversal potential, because the I_{test}-V_{pre} relation obtained with Ba^{2+} as the charge carrier is identical to that with Ca^{2+} (Fig. 2 *B*, *open symbols*), apart from a surface-potential shift. The properties of recombinant N-type channel inactivation are clearly incongruent with the profiles of "classic" voltage-dependent or calcium-sensitive inactivation.

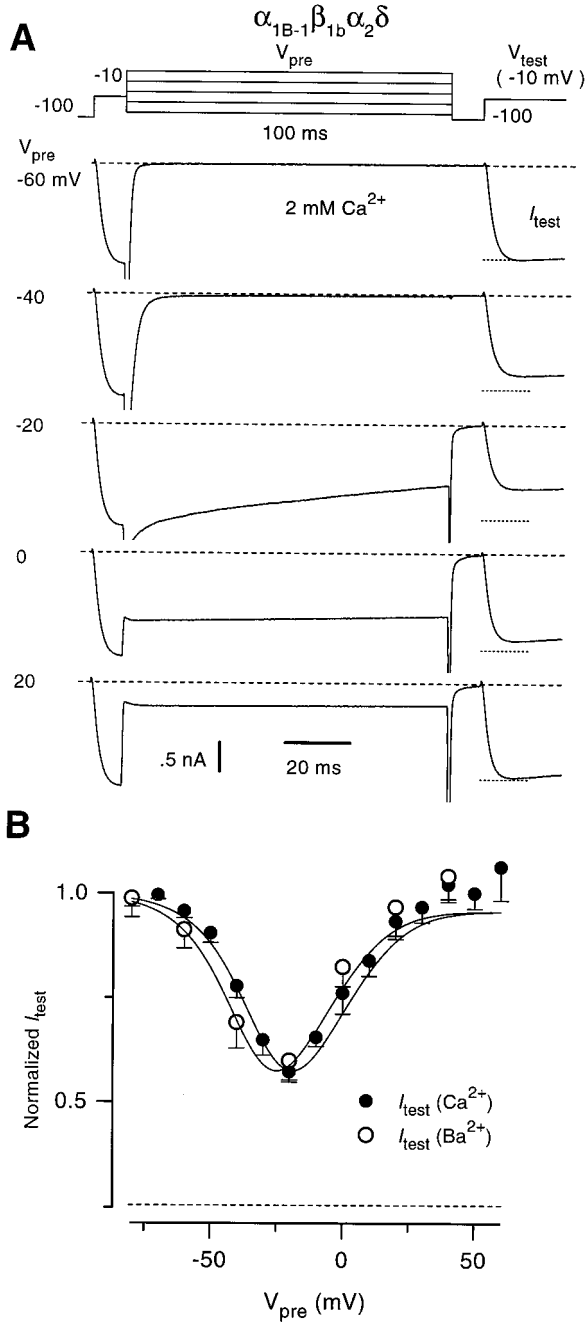

FIGURE 2 Effect of prepulses on the availability of ionic current. (*A*) Prepulse inactivation of test pulse ionic currents, illustrating that inactivation bears a U-shaped dependence upon prepulse voltage. Prepulse voltages corresponding to various traces are labeled on the left. Currents were recorded with 2 mM Ca^{2+} as a charge carrier. Data are from cell 378_5, transfected with $\alpha_{1B\text{-}1}$ β_{1b} $\alpha_2\delta$. (*B*) Plot of normalized, test pulse current versus prepulse potential (I_{test}-V_{pre}), measured with either 2 mM Ca^{2+} (*solid circles*, n = 14–18) or 2 mM Ba^{2+} (*open circles*, n = 4) as the charge carrier, illustrating that the I_{test}-V_{pre} relation has a similar U-shape in the two solutions. Apart from a 6-mV shift, the same fit (*solid lines*) is used for two sets of data.

To obtain an initial assessment of the effects of inactivation on gating-charge movement, we performed a similar prepulse experiment, but now with test depolarization to the reversal potential for ionic current (~45 mV). This variant

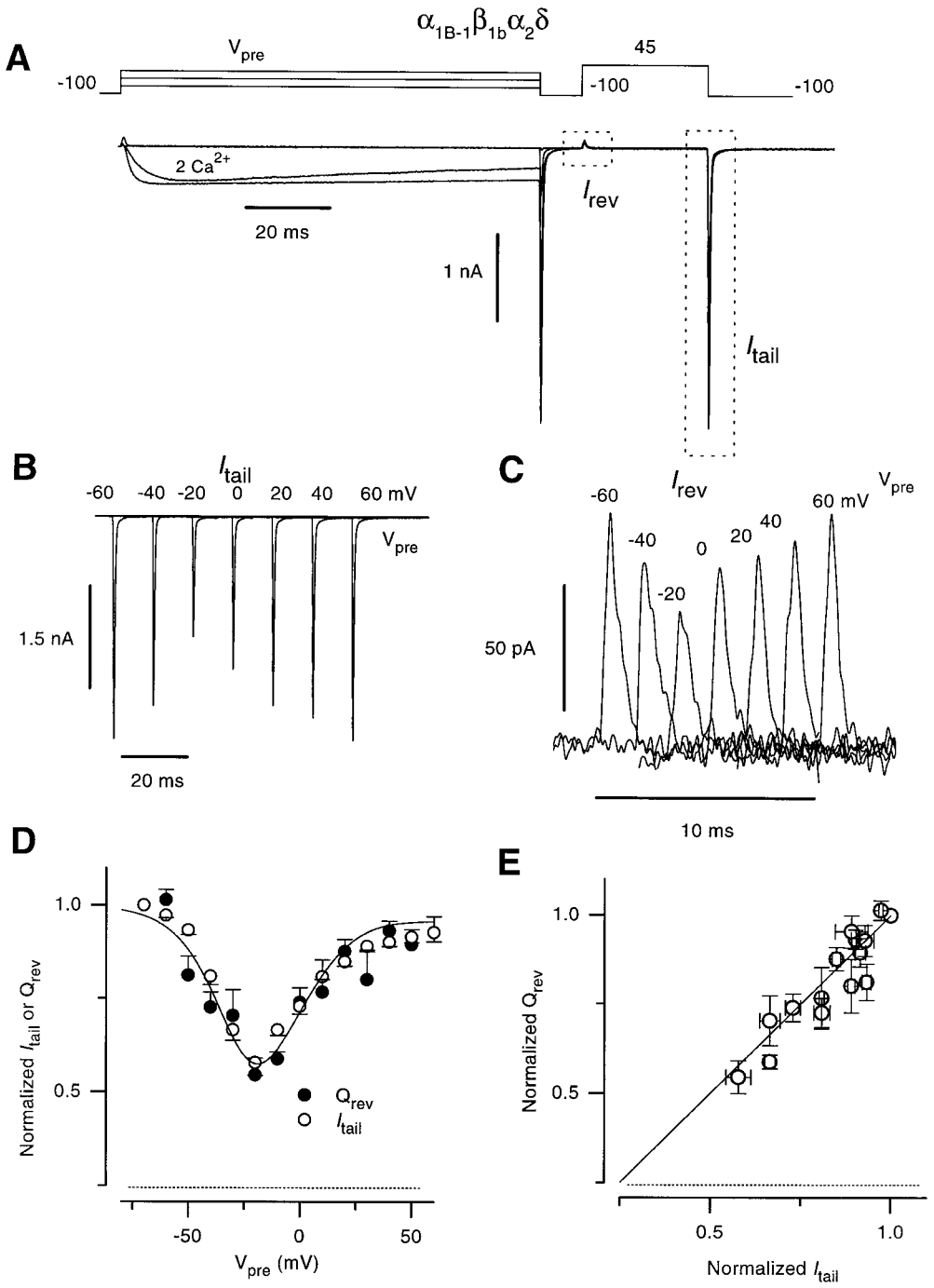

FIGURE 3 Effect of prepulses on currents measured at the reversal potential for ionic current. (*A*) Whole-cell currents measured in 2 mM Ca^{2+}, for cell 355_5, transfected with α_{1B-1} β_{1b} $\alpha_2\delta$. The prepulse protocol (*top*) is similar to that in Fig. 2 *A*, except that the test pulse potential is set to the reversal potential for ionic current. This allows correlative examination of prepulse effects on putative gating currents (I_{rev}) and ionic tail currents (I_{tail}). Displayed traces are for V_{pre} equal to −40, −20, 0, and 40 mV. (*B*, *C*) Close-up view of putative test pulse gating currents (I_{rev}) and test pulse tail currents (I_{tail}), for the indicated prepulse potentials. Prepulses produce similar effects on these quantities. (*D*) Comparison of prepulse effects on the availability of gating charge mobility (Q_{rev}-V_{pre}, *closed circle*) and ionic current (I_{tail}-V_{pre}, *open circle*). Q_{rev} was derived by integrating I_{rev}. The data points for V_{pre} = −80 mV were used to normalize data before averaging across cells (n = 4–8). The fit is reproduced from Fig. 2 *B*. (*E*) One-to-one correlation between the availability of ionic current (I_{tail}) and gating charge (Q_{rev}). Data from *D* are plotted versus one another, with each point corresponding to a single prepulse potential. The line of identity is plotted for reference.

of the prepulse-inactivation protocol (Fig. 3 *A*) promises to permit simultaneous measurements of ionic current inactivation and gating currents, as follows. The extent of prepulse inactivation can be gauged from the decrement of tail currents after the brief test pulse (I_{tail}). With regard to gating currents, ionic currents should, in principle, vanish at the

reversal potential, leaving behind gating currents arising from voltage-sensor movement (I_{rev}). Here the integral of I_{rev} (Q_{rev}) should be equal to the maximum amount of mobile gating charge, because N-type channels fully activate by +45 mV (Jones et al., 1997, and below). Visual inspection of such aligned test-pulse responses suggests that prepulse inactivation of ionic currents (I_{tail} in Fig. 3 *B*) parallels reduction of presumed gating current (I_{rev} in Fig. 3 *C*). In fact, quantitative comparison of I_{test} and Q_{rev} (Fig. 3, *D* and *E*) reveals that prepulse inactivation of ionic current correlates one to one with the reduction in Q_{rev}. If I_{rev} is genuine gating current, then this experiment suggests that N-type channel inactivation produces essentially complete gating charge immobilization (Armstrong and Bezanilla, 1977).

According to precedent in other voltage-gated channels, gating charge immobilization would suggest that N-type channel inactivation is voltage dependent (Armstrong, 1981; Bezanilla, 1985). However, despite the strong historical link between gating charge immobilization and voltage-dependent inactivation in other channels, it could be that the presumed immobilization in N-type channels (Fig. 3) results from an unusual form of current-dependent inactivation that both induces gating charge immobilization and senses Ca^{2+} and Ba^{2+} equally. To distinguish between these possibilities, we sought to examine prepulse effects on gating currents isolated during complete blockade of ionic current. This experimental configuration would eliminate any current-dependent contribution to inactivation and charge immobilization. In addition, such blockade would also permit unambiguous resolution of gating current, enabling verification that I_{rev} currents (Fig. 3 *C*) are actual gating currents.

Although we have recently shown that La^{3+} could be used to block rat α_{1B} ionic currents, (Dubel et al., 1992; Jones et al., 1997), in this paper we use the human $\alpha_{1B\text{-}1}$ clone (Williams et al., 1992). Therefore, as a prerequisite to such experiments, we first demonstrate that La^{3+} blockade of ionic current produces the desired isolation of human $\alpha_{1B\text{-}1}$ gating currents, without artifactual distortion of voltage-sensor movement (Kamp et al., 1996). These results are summarized in Fig. 4, using the β_{2a} auxiliary subunit to slow inactivation (Patil et al., 1998) and thereby facilitate examination of gating charge properties associated with activation alone.

Fig. 4 *A* shows current records during the first 5 ms of test depolarizations to various potentials, obtained before (*dashed lines*) and after (*solid lines*) ionic current blockade. The transient outward current in both sets of traces fits the profile of a gating current arising from voltage sensor movement that precedes ionic current activation. Therefore, the invariance of the initial portion of this transient upon La^{3+} blockade argues that La^{3+} does not distort voltage sensor movement. Likewise, our interpretation of I_{rev} (Fig. 3) as a genuine gating current is supported by the absence of any effect of La^{3+} blockade upon the outward transient at the reversal potential (~45 mV).

Further evidence that the transients during La^{3+} block are actual gating currents comes from the voltage-dependent behavior of such currents (Fig. 4 *B*), especially in relation to the voltage-dependent activation of ionic current (Fig. 4 *C*). First, the time integrals of outward current transients (Q_{on}) are closely similar to the time integrals of ensuing inward current transients (Q_{off}), and both entities saturate together with increasing depolarization (Fig. 4 *D*), all as expected for charge associated with voltage sensors trapped in the membrane. Here, using β_{2a} simplifies the comparison of Q_{on} and Q_{off} by eliminating the need to consider the effects of test-pulse inactivation on voltage sensor movement. Second, as expected for charge movement that is linked to channel (de)activation, Q_{on}-V and Q_{off}-V (Fig. 4 *D*) rise before and then parallel activation of ionic current, here represented by the G-V curve (Fig. 4 *D*) derived from tail currents (Fig. 4 *C*). No relative surface potential correction is required in the comparison of Q-V and G-V curves, because the invariance of early outward transients upon La^{3+} blockade (Fig. 4 *A*) indicates little or no change in surface potential between solutions used for recording ionic (2 mM Ca^{2+}) and gating currents. Finally, consistent with gating currents arising from active (conducting) channels, the maximum amount of gating charge (Q_{max}) is linearly correlated with peak ionic current density (Fig. 4 *E*). Here, Q_{max} is obtained from integration of the maximum charge at the reversal (~+45 mV). Results analogous to those in Fig. 4 (*A–E*) were obtained with channels containing β_{1b} or β_3 auxiliary subunits, as illustrated by the similarity of Q_{on}-V and G-V curves with different β-subunits (Fig. 4 *F*). Similar insensitivity of Q-V and G-V curves to the type of β-subunit was also reported for neuronal α_{1E} calcium channels (Jones et al., 1998). The results in Fig. 4, along with other technical prerequisites described in Materials and Methods (Fig. 1), validate the use of La^{3+} blockade to resolve human $\alpha_{1B\text{-}1}$ gating currents and their modulation by inactivation.

Fig. 5 *A* illustrates the effect of prepulse depolarization on N-type channel ($\alpha_{1B\text{-}1}$ β_{1b} $\alpha_2\delta$) gating currents, here isolated by La^{3+} blockade. The prepulse inactivation protocol shown at the top is analogous to that used for experiments with ionic current (Figs. 2 *A* and 3). As in experiments where gating current was isolated only by depolarizing to the reversal potential in 2 mM Ca^{2+} (Fig. 3), increasing the prepulse voltage first reduces and then increases the test pulse gating current. This behavior results in a U-shaped relation between test pulse gating charge and prepulse potential (Fig. 5 *B*, $Q_{on,test}$-V relation, *filled circles*), which appears to be indistinguishable from the analogous Q_{rev}-V measured in 2 mM Ca^{2+} (Fig. 5 *B*, *open circles* reproduced from Fig. 3 *D*). A plot of $Q_{on,test}$ as a function of Q_{rev} falls on the line of identity (Fig. 5 *C*), which confirms that the extent of gating charge immobilization is unaffected by the presence or absence of ionic current during the prepulse. These results demonstrate that prepulse effects on voltage sensor movement are exclusively mediated by voltage-dependent processes.

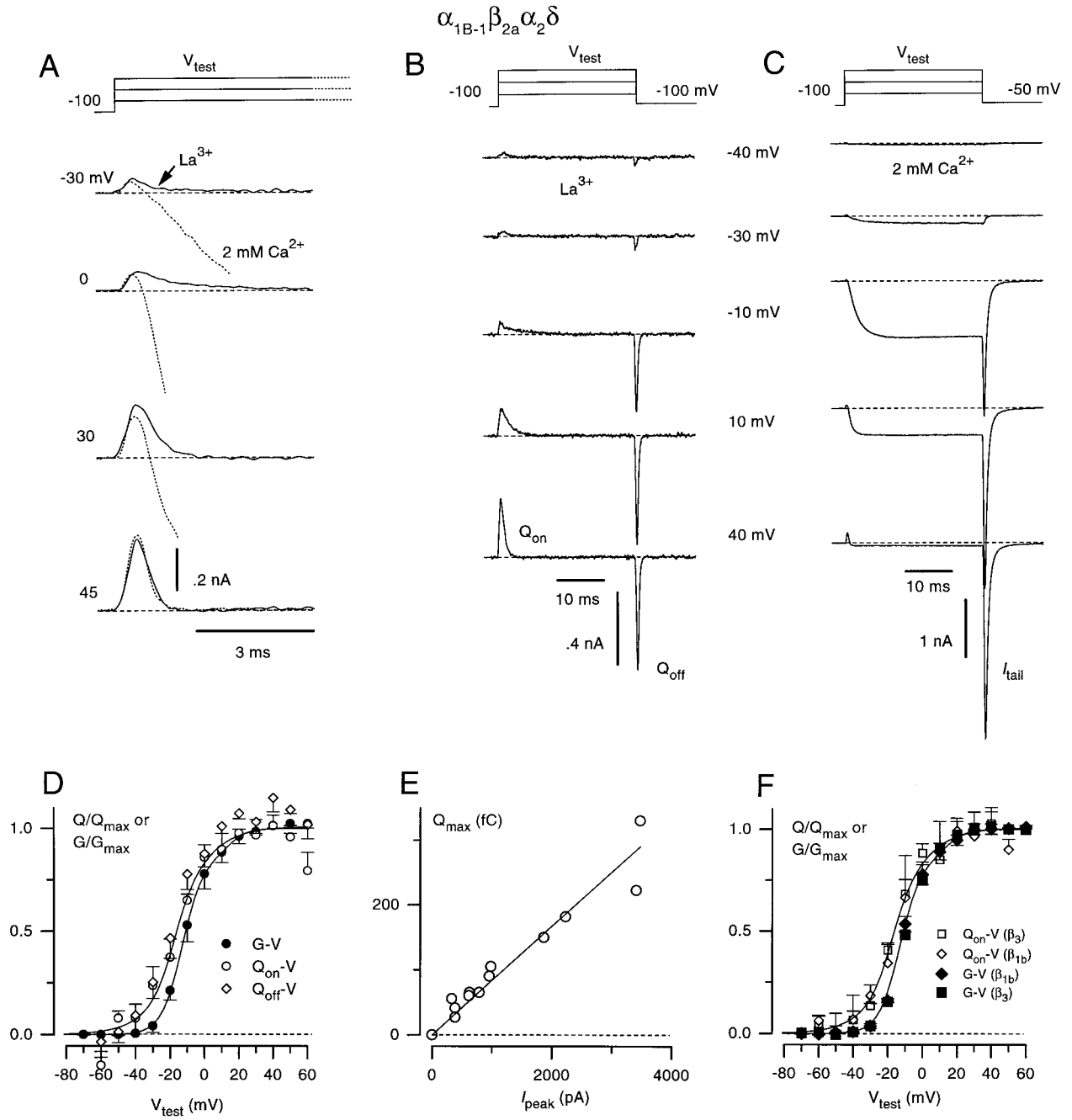

FIGURE 4 Measurement of gating currents during ionic current blockade with 2 mM Mg^{2+}/0.2 mM La^{3+}. (*A*) Whole-cell currents are shown for the first 5 ms of depolarization to the indicated potentials, all from a holding potential of −100 mV. The initial outward transient should be dominated by gating current. For each test potential, the current measured in 2 mM Ca^{2+} (*dotted line*) is superimposed on the current measured during La^{3+} blockade (*solid line*) to demonstrate that La^{3+} does not alter gating charge movement. Data are for cell 340_2, transfected with α_{1B-1} β_{2a} $\alpha_2\delta$. (*B*) Slower time base plots of whole-cell currents elicited upon depolarization and repolarization, all during La^{3+} blockade. Such responses were used to determine the voltage dependence of gating charge movement, as gauged by *Q-V* curves shown below (*D*, *F*). Data are from cell 360_3. (*C*) Ionic currents recorded in 2 mM Ca^{2+}, elicited by the voltage protocol (*top*) used for determining the voltage dependence of ionic current activation, as characterized by *G-V* curves shown below (*D*, *F*). Data are from cell 363_8. (*D*) Comparison of the voltage dependence of gating charge movement (*Q-V*) to the voltage dependence of ionic current activation (*G-V*). *Q-V* curves were derived from integrating the transient during depolarization (Q_{on}-*V*, *open circle*, $n = 4$) or repolarization (Q_{off}-*V*, *open diamond*) and normalizing by an estimate for the maximum amount of mobile charge (see Materials and Methods). The voltage dependence of ionic activation (*G-V*, *closed circle*, $n = 5$) was calculated from tail currents upon repolarization to −50 mV, after normalization by an estimate of the maximum tail current (see Materials and Methods). Solid lines correspond to dual Boltzmann fits. Parameters for the *Q-V* fit were $f_{low} = 0.39$, $z_{low} = 4.7$, $V_{low} = -17.9$ mV, $f_{high} = 0.63$, $z_{high} = 1.98$, $V_{high} = -13.2$ mV. Parameters for the *G-V* fit were $f_{low} = 0.86$, $z_{low} = 4.2$, $V_{low} = -12.9$ mV, $f_{high} = 0.14$, $z_{high} = 4.8$, $V_{high} = 14$ mV. (*E*) Linear correlation between the maximum mobile gating charge (Q_{max}), taken as the gating charge moved in response to a 45-mV depolarization, and the peak test pulse current (I_{peak}). Each data point represents one cell. The line represents a fit by eye. (*F*) Superposition of Q_{on}-*V* and *G-V* relations for channels containing β_3 (Q_{on}-*V*, *open square*, $n = 3$; *G-V*, *filled square*, $= 1$) and channels containing β_{1b} (Q_{on}-*V*, *open diamond*, $n = 5$; *G-V*, *filled diamond*, $n = 5$). Fits are reproduced from *D*.

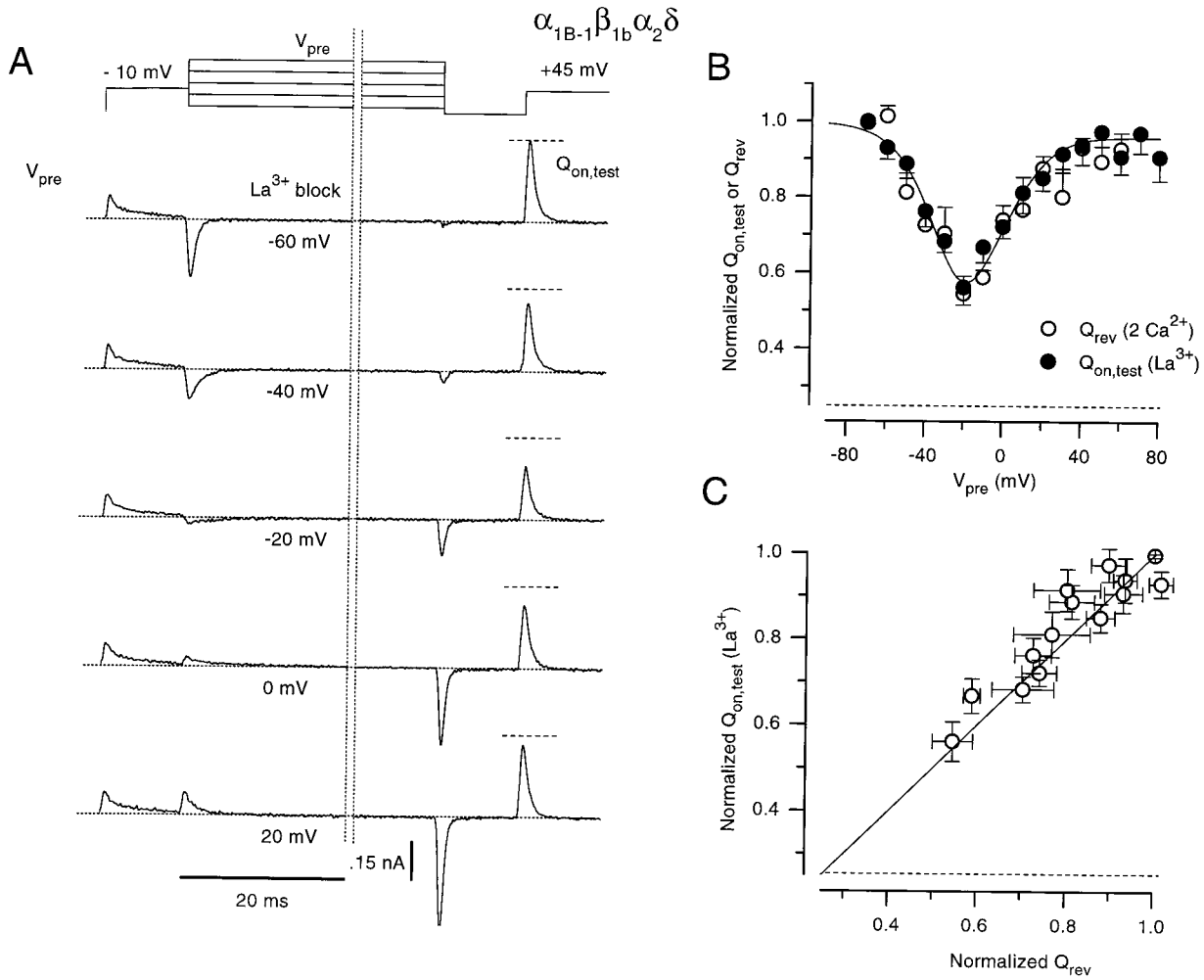

FIGURE 5 Prepulse effects on gating charge movement during La^{3+} blockade. (*A*) Gating currents measured from cell 367_1, transfected with α_{1B-1} β_{1b} $\alpha_2\delta$. The prepulse protocol (*top*) is identical to that in Fig. 2 *A* (prepulse duration of 100 ms), except that the test pulse potential is +45 mV, to measure the maximum amount of mobile gating charge. The horizontal dashed line indicates the maximum value of the test pulse gating current, as measured after a prepulse to −60 mV. An axis break (*vertical dotted lines*) was included to permit an optimal display time base for visual resolution of gating currents. The time scale bar pertains to both sides of the axis break. (*B*) Comparison of prepulse effects on availability of test pulse gating charge during La^{3+} blockade ($Q_{on,test}$-V_{pre}, *filled circles*, n = 11–21) versus availability of test pulse gating charge measured in 2 mM Ca^{2+} (Q_{rev}-V_{pre}, *open circles*, data reproduced from Fig. 3 *D*). In general, different cells were used to obtain $Q_{on,test}$ and Q_{rev}. Data were normalized by the value of the data point for V_{pre} = −80 mV, before averaging across cells. The solid line is the fit from Fig. 2 *B*. (*C*) One-to-one correlation between normalized Q_{rev} and normalized $Q_{on,test}$ (both from *B*), with each data point corresponding to one prepulse potential. The line of identity is plotted for reference. This correlation illustrates that the extent of gating charge immobilization was the same, regardless of the influx of ionic current during prepulses.

Because the properties of gating current were essentially identical in La^{3+} and Ca^{2+}, we were justified in correlating gating current data measured with La^{3+} blockade (Fig. 5) with ionic current data measured in 2 mM Ca^{2+} (Fig. 2). This offered a technical advantage in that gating currents measured during La^{3+} blockade routinely permitted superior resolution of charge movement. Fig. 6 summarizes the results of the comparison for α_{1B-1} β_{1b} $\alpha_2\delta$. Expanded-time base records of test pulse ionic (Fig. 6 *A*) and gating (Fig. 6 *B*) currents, derived from previously described prepulse inactivation experiments (Figs. 2 *A* and 5 *A*, respectively), visually underscore the U-shaped voltage dependence of ionic current inactivation and gating charge immobilization upon prepulse depolarization. Further comparison of the average extent of ionic current inactivation and gating charge reduction (Fig. 6, *C* and *D*, data from Figs. 2 *B* and 5 *B*) reiterates the close correlation seen in Fig. 3 *D*, in which gating currents were measured at the ionic current reversal potential in 2 mM Ca^{2+} (Fig. 3 *D*). The presence of this one-to-one relationship between ionic current inactivation and gating charge immobilization under both conditions (with and without ionic current block; compare Figs. 3 *E* and 6 *D*) implies that the N-type channel inactivation seen here is purely voltage dependent and results in complete immobilization of voltage sensor movement over the range of activation.

To provide further evidence for the one-to-one linkage between inactivation and charge immobilization, we examined their correlation in protocols with variable prepulse

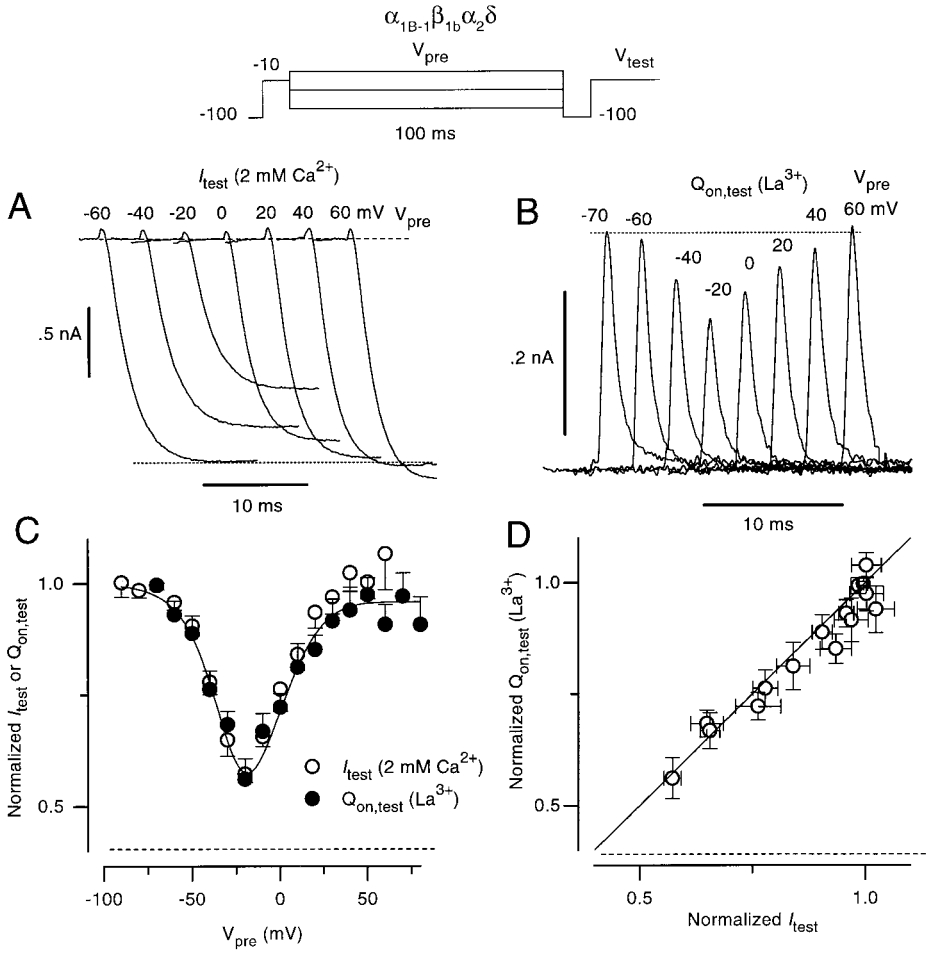

FIGURE 6 Explicit comparison of prepulse effects on ionic current (measured in 2 mM Ca^{2+}) and on gating currents (recorded during La^{3+} blockade). All data are from cells with α_{1B-1} β_{1b} $\alpha_2\delta$ channels. (*A*, *B*) Expanded view of test pulse ionic currents (*A*, V_{test} = −10 mV) and gating currents (*B*, V_{test} = +45 mV) for the cells in Figs. 2 *A* and 5 *A*, respectively. These illustrate that ionic and gating currents are affected to a similar degree by prepulses. (*C*) Comparison of the I_{test}-V_{pre} relation from Fig. 2 *B* to the $Q_{on,test}$-V_{pre} relation from Fig. 5 *B*, demonstrating that gating charge and ionic current exhibit a similar U-shaped dependence on prepulse potential. The solid line is a fit from Fig. 2 *B*. (*D*) One-to-one correlation between $Q_{on,test}$ and I_{test} (both from *C*), with each point corresponding to a particular prepulse potential. The close approximation of data to the line of identity demonstrates essentially identical prepulse effects on the availability of ionic current and mobile gating change.

duration and in experiments in which channel subunit composition was changed. Fig. 7 illustrates the effect of varying the duration of a prepulse on test pulse ionic and gating currents. Clearly, prepulses of increasing duration result in a parallel decrease in both test pulse ionic current (Fig. 7 *A*) and test pulse gating current (Fig. 7 *B*). Again, ionic current inactivation and gating charge immobilization develop simultaneously, in a directly proportional manner (Fig. 7, *C* and *D*). The tight correlation in this kinetic experiment suggests that the induction of gating charge immobilization and the induction of ionic current inactivation are functional manifestations of the same molecular event. Otherwise, if gating charge immobilized in a step after ionic inactivation, the time course of charge immobilization would be delayed with respect to ionic current inactivation (Nonner, 1980).

Because coassociation with different calcium channel β-subunits results in N-type calcium channels with widely varying inactivation properties (Patil et al., 1998), we replicated the prepulse inactivation protocols already performed on α_{1B-1} β_{1b} $\alpha_2\delta$ channels (Fig. 6), using slower-inactivating (α_{1B-1} β_{2a} $\alpha_2\delta$) and faster-inactivating (α_{1B-1} β_3 $\alpha_2\delta$) N-type channels. These experiments illustrate that the relationship between gating charge immobilization and ionic current inactivation is similar in channels of differing molecular composition. Figs. 8 (α_{1B-1} β_{2a} $\alpha_2\delta$) and 9 (α_{1B-1} β_3 $\alpha_2\delta$) show the results of the experiments, following nearly the identical format used for α_{1B-1} β_{1b} $\alpha_2\delta$ channels (Figs. 2, 5, and 6). The slow inactivation of α_{1B-1} β_{2a} $\alpha_2\delta$ channels is apparent in Fig. 8, so that 100-ms prepulses no longer have much effect on either test pulse ionic (Fig. 8, *A* and *C*) or gating (Figs. 8, *B* and *D*) currents. As expected, the prepulse inactivation relation for ionic current (Fig. 8 *E*, I_{test}-V_{pre}) is flattened, reflecting the reduced inactivation rate. On the other hand, channels containing the β_3-subunit inactivate more rapidly than channels containing β_{1b}, such that the dip and upturn of the prepulse inactivation relation for ionic current are enhanced (Fig. 9 *E*). Here, even with the sharpest minimum in the prepulse inactivation curve, we consider this relation to reflect kinetic properties of inactivation, because steady-state inactivation is nearly complete for voltages ≥−40 mV (Fig. 9 *E*, *diamonds*). With either β_{2a} or β_3, the degree of gating charge immobilization is directly proportional to the extent of ionic current inactivation (Figs. 8 *E*, 8 *F*, 9 *E*, 9 *F*).

DISCUSSION

We have correlated the inactivation of ionic currents with a reduction in the gating currents of N-type calcium channels.

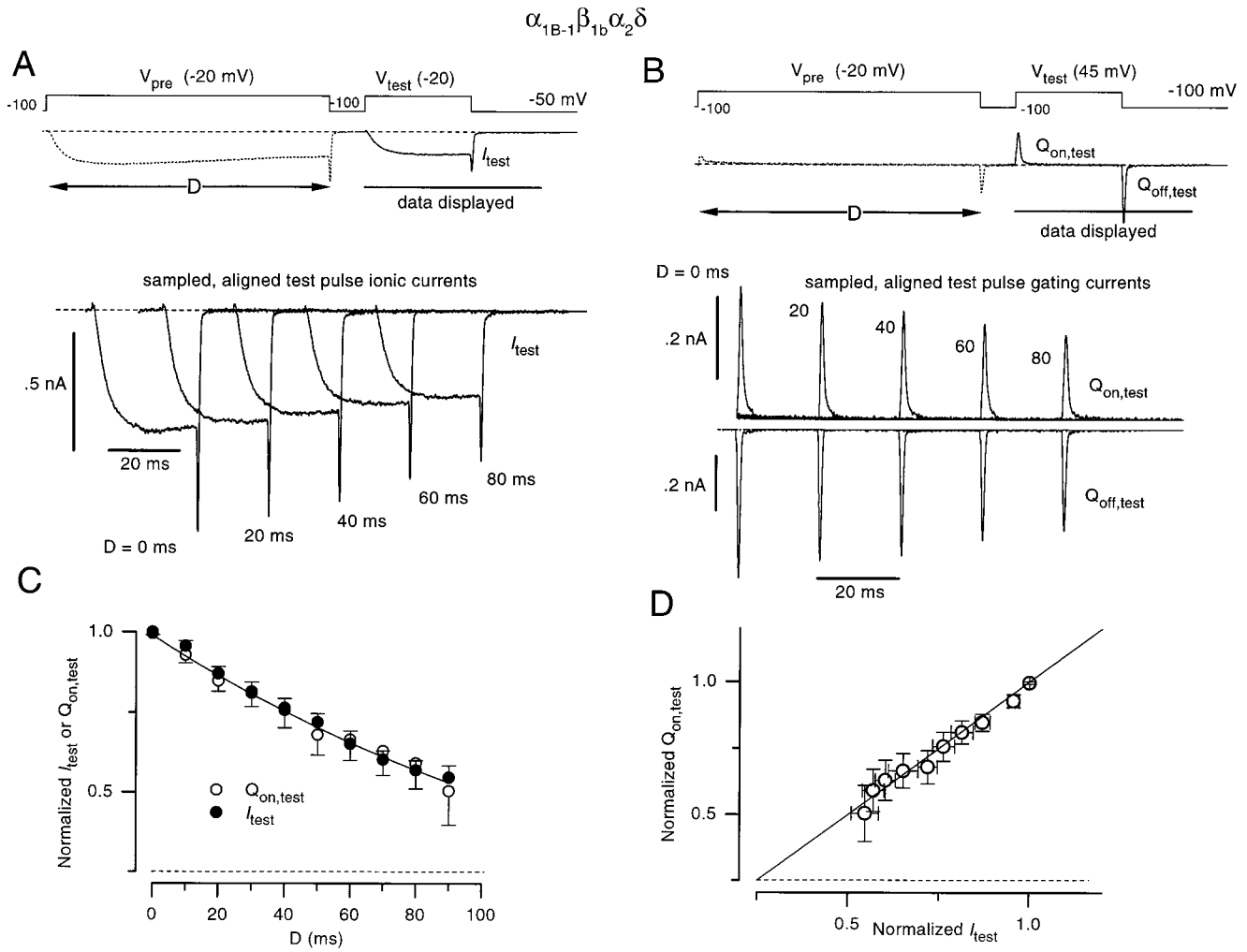

FIGURE 7 Comparison of the kinetics of ionic current inactivation and gating charge immobilization, for cells transfected with α_{1B-1} β_{1b} $\alpha_2\delta$. (*A*, *Top*) Variable-duration prepulse protocol, as illustrated by the voltage protocol and representative ionic current trace. The solid horizontal bar under I_{test} marks the region of traces displayed below on an expanded time base. The portion of the trace plotted as a solid curve also corresponds to the region chosen for expanded time base display. (*Bottom*) Aligned test pulse ionic currents (I_{test}) measured in 2 mM Ca^{2+} after a prepulse to −20 mV for the indicated duration. All data are from cell 372_2. (*B*) Gating currents measured during La^{3+} blockade. The voltage protocol is identical to that in *A*, except with a test pulse potential of +45 mV instead of −20 mV. The test pulse "on" and "off" transients for a given prepulse duration are aligned. All data are from cell 372_6. (*C*) Comparison of the time course of ionic current inactivation (I_{test}, *filled circle*, $n = 7$) and gating charge immobilization ($Q_{on,test}$, *open circle*, $n = 7$). I_{test} and $Q_{on,test}$ are normalized by their respective values without a prepulse. The exponential fit ($\tau = 158$ ms) was drawn by eye. (*D*) One-to-one correlation between inactivation of ionic current (I_{test}) and gating charge ($Q_{on,test}$). Data are from *C*, with each data point corresponding to one prepulse duration. The line of identity is drawn for reference.

Such gating charge "immobilization" (Armstrong and Bezanilla, 1977) provides evidence that N-type channel inactivation occurs by a purely voltage-dependent process, despite the U-shaped voltage dependence of inactivation that is generally considered a hallmark of current-dependent inactivation (Brehm and Eckert, 1978). The argument is summarized as follows. By precedent in other channels, inactivation-related immobilization argues against a current-dependent mechanism (Hadley and Lederer, 1991b; Shirokov et al., 1993). But the evidence here for voltage-dependent inactivation is even more direct. Prepulse-induced immobilization of gating charge is similar in the absence and presence of ionic current blockade (Fig. 5 *C*), which implies that the effects on gating charge are purely voltage dependent. Furthermore, the one-to-one correspondence between reduction of gating charge and ionic current inactivation (Figs. 3 *E*, 5 *C*, 6 *D*) strongly suggests that these two phenomena reflect the same underlying molecular event. Hence, we argue that the ionic current inactivation arises from a solely voltage-dependent mechanism. This proposal is also supported by the insensitivity of ionic current inactivation to changes in charge carrier and intracellular Ca^{2+} buffering observed with human N-type (α_{1B-1}) channels expressed in HEK 293 cells (McNaughton and Randall, 1997; Patil et al., 1998).

With attention appropriately focused on voltage-dependent processes, the subsequent sections of the discussion explore the implications of our results for the mechanism of

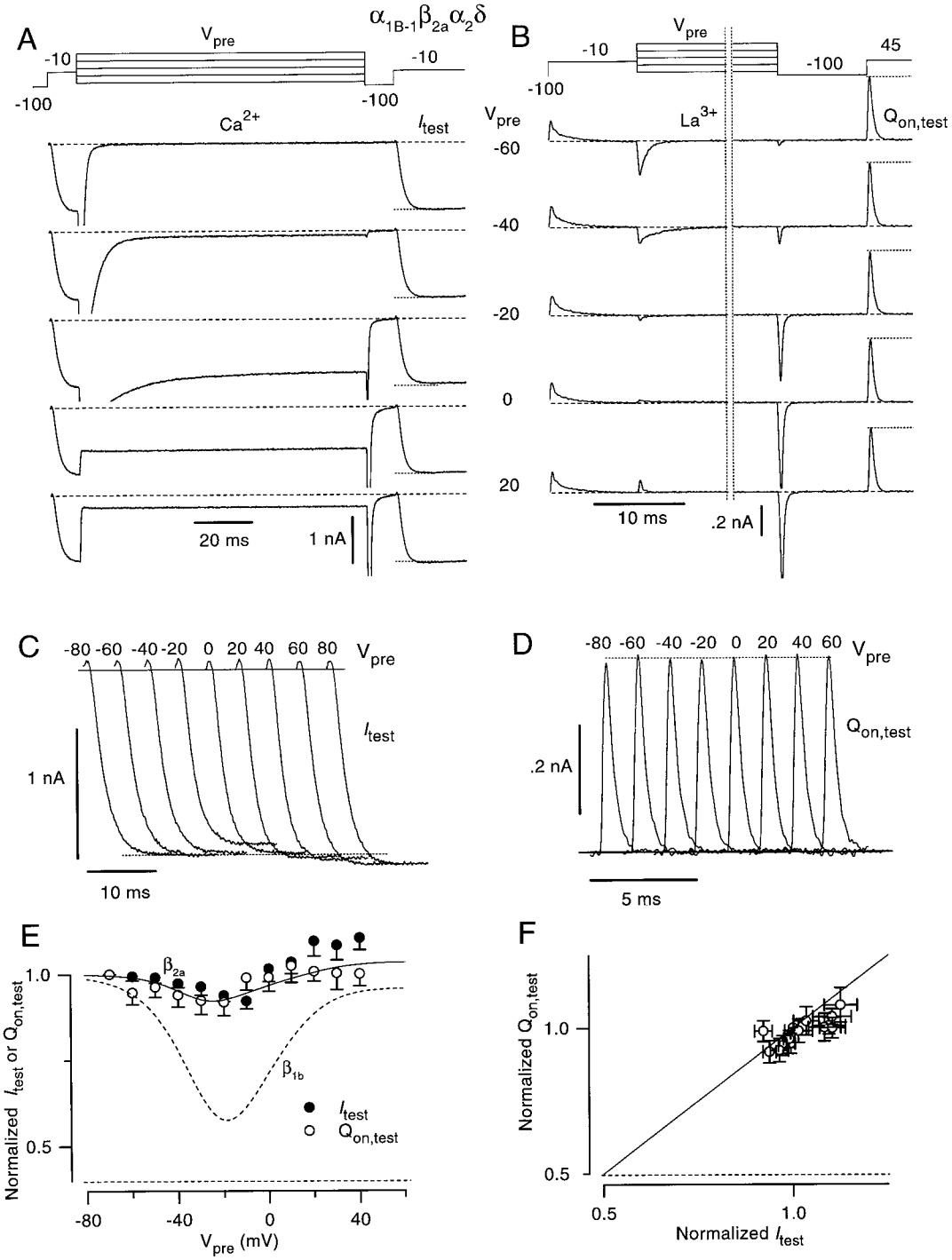

FIGURE 8 Prepulse effects on ionic currents (measured in 2 mM Ca^{2+}) and gating currents (recorded during La^{3+} blockade), for α_{1B-1} β_{2a} $\alpha_2\delta$ channels. (*A*, *B*) Exemplar ionic currents (*A*, cell 344_1) and gating currents (*B*, cell 347_1) elicited by voltage protocols (*top*) analogous to those used in Figs. 2 *A* and 5 *A*, respectively. Note the reduced effect of prepulses on both ionic and gating currents, compared to channels containing β_{1b}. (*C*, *D*) Close-up of test pulse ionic (*C*) and gating (*D*) currents after prepulses to the indicated potentials. Data are from corresponding cells in *A* and *B*. (*E*) Comparison of prepulse effects on the availability of ionic current (I_{test}, *filled circle*, $n = 6–8$) and the maximum amount of mobile gating charge ($Q_{on,test}$, *open circle*, $n = 8–9$). *For reference*, *the dashed line reproduces the fit to* β_{1b} *data in Fig.* 2 *B*. (*F*) One-to-one correlation of $Q_{on,test}$ and I_{test}. Data replotted from *E*, with each symbol corresponding to one prepulse potential. The line of identity is shown for reference.

N-type channel inactivation. First, we assess the quantitative reliability of the data. Second, we review prevailing models of voltage-dependent inactivation in potassium and sodium channels, thereby providing a conceptual framework for understanding N-type calcium channel inactivation. Third, we evaluate N-type channel behavior against the

backdrop of such prevailing models, to highlight distinctions of N-type channel inactivation, as well as commonalities that may reflect similarities in underlying molecular mechanism. We develop analytic arguments to show that the distinguishing characteristics of N-type channel inactivation imply that inactivation occurs preferentially from intermediate closed states along the activation pathway. Fourth, we formulate specific features of such "preferential closed-state inactivation" (PCSI) mechanisms, which collectively emerge as constraints from all of the experimental results. Finally, we consider the generalizability of our deductions to N-type channel behavior in native neurons.

Authenticity of inactivation-related changes in gating current

Accurate measurements of the extents of ionic current inactivation and gating charge immobilization figure importantly in our attempts to infer mechanism. We already have excluded gating current distortion owing to leak subtraction artifacts (Fig. 1, Materials and Methods). Here we consider two further technical issues.

The first concerns the possibility that part of the prepulse-induced change in test pulse current is related to voltage-dependent relief of basal G-protein inhibition (called "prepulse facilitation," as in Grassi and Lux (1989)) and not solely to inactivation. Although we minimized G-protein activation through dialysis with GDPβS (Ikeda, 1991), a hint of such facilitation is still apparent upon close examination of Figs. 6 *A* and 8 *C*, where prepulses to potentials greater than 20 mV actually enhance the exemplar test current slightly relative to the control. However, on average the degree of facilitation is a few percent at most, for the following reasons. First, any increase in test pulse current from relief of G-protein inhibition should be much less evident at +45 mV versus −10 mV (Bean, 1989); yet prepulses have similar effects on test pulse currents at either voltage (compare Fig. 3 *D* to Fig. 2 *B*). Second, because the total amount of mobile gating charge (Q_{max}) is not subject to G-protein modulation (Jones et al., 1997), any increase in test pulse current from relief of G-protein inhibition should be uncorrelated with an increase in Q_{max}. Yet, the $Q_{on,test}$-V_{pre} and I_{test}-V_{pre} relations are remarkably similar (Fig. 6 *C*). Only the difference of a few percent seen near saturating depolarization may be attributable to facilitation.

The second technical point regards the extent to which gating current is isolated from ionic current. In the case of perfect isolation of gating current, the integrals of "on" and "off" gating currents should be equal. However, as evident in Fig. 4 *D*, Q_{off} is ~10% larger than Q_{on} across most of the voltage range. This discrepancy likely reflects a small degree of ionic current breakthrough in the "off" transient, because the addition of 2 μM ω-conotoxin GVIA (ω-CTX) nearly abolishes the difference between Q_{off} and Q_{on} (data not shown). On the other hand, isolation of "on" gating currents is excellent, because currents obtained during La^{3+} blockade uniformly decayed to zero by the end of test pulse depolarization. Accordingly, our quantitative analysis and inference are limited to Q_{on}.

Prevailing forms of voltage-dependent inactivation in potassium and sodium channels

Inactivation was originally proposed as a single, intrinsically voltage-dependent process that was entirely independent of activation (Hodgkin and Huxley, 1952). By contrast, the current view of potassium and sodium channels now includes two or more dominant forms of inactivation, generally considered intrinsically voltage insensitive, but coupled to voltage-dependent activation. Fig. 10 provides a working summary of the main forms in terms of structural, kinetic, and gating current perspectives. Although this synopsis of ongoing work is certainly subject to revision and debate, it nonetheless serves as a valuable framework for subsequent consideration of N-type calcium channel inactivation.

In "N-type" inactivation of potassium channels (Hoshi et al., 1990), a tethered ball plugs the cytoplasmic mouth of the open channel (Zagotta et al., 1990) to produce inactivation (Fig. 10 *A*, *left*). When the channel engages the inactivation ball, it appears that some of the S4 voltage sensors cannot return to their fully resting position, because channels that inactivate during a strong depolarizing step return only a fraction of their total gating charge in the usual fast component of "off" gating current (Bezanilla et al., 1991). The remainder of the total gating charge is "immobilized" (Armstrong and Bezanilla, 1977) and returns as an unusually slow kinetic component that probably reflects gradual recovery from inactivation. Such interaction between activation (S4 voltage sensor movement) and inactivation violates the independence prediction of Hodgkin and Huxley (Armstrong, 1981; Bezanilla, 1985) and strongly supports coupling between inactivation and activation, as illustrated by the state diagram (Fig. 10 *A*, *middle*). The overall features of the kinetic scheme, including voltage-insensitive vertical transitions to and from inactivation, are supported not only by gating current experiments, but also by a spectrum of ionic current protocols (Zagotta et al., 1989; Zagotta and Aldrich, 1990; Demo and Yellen, 1991). The absence of inactivated states (I) beneath the leftmost closed (C) states reflects the restriction of inactivation to the full return of S4 sensors. Although such "missing" I states may exist, we omit them from the state diagram, because there is no direct gating current evidence that they can be appreciably populated. Inactivated channels can, however, undergo rapid, voltage-dependent transitions among an incomplete complement of inactivated (I) states, accounting for the partial return of total gating charge as a fast component of "off" gating current. With prolonged repolarization, inactivated channels appear to further undergo a rate-limiting upward step (recovery from inactivation), followed by rapid voltage-dependent transitions through the left half of C states.

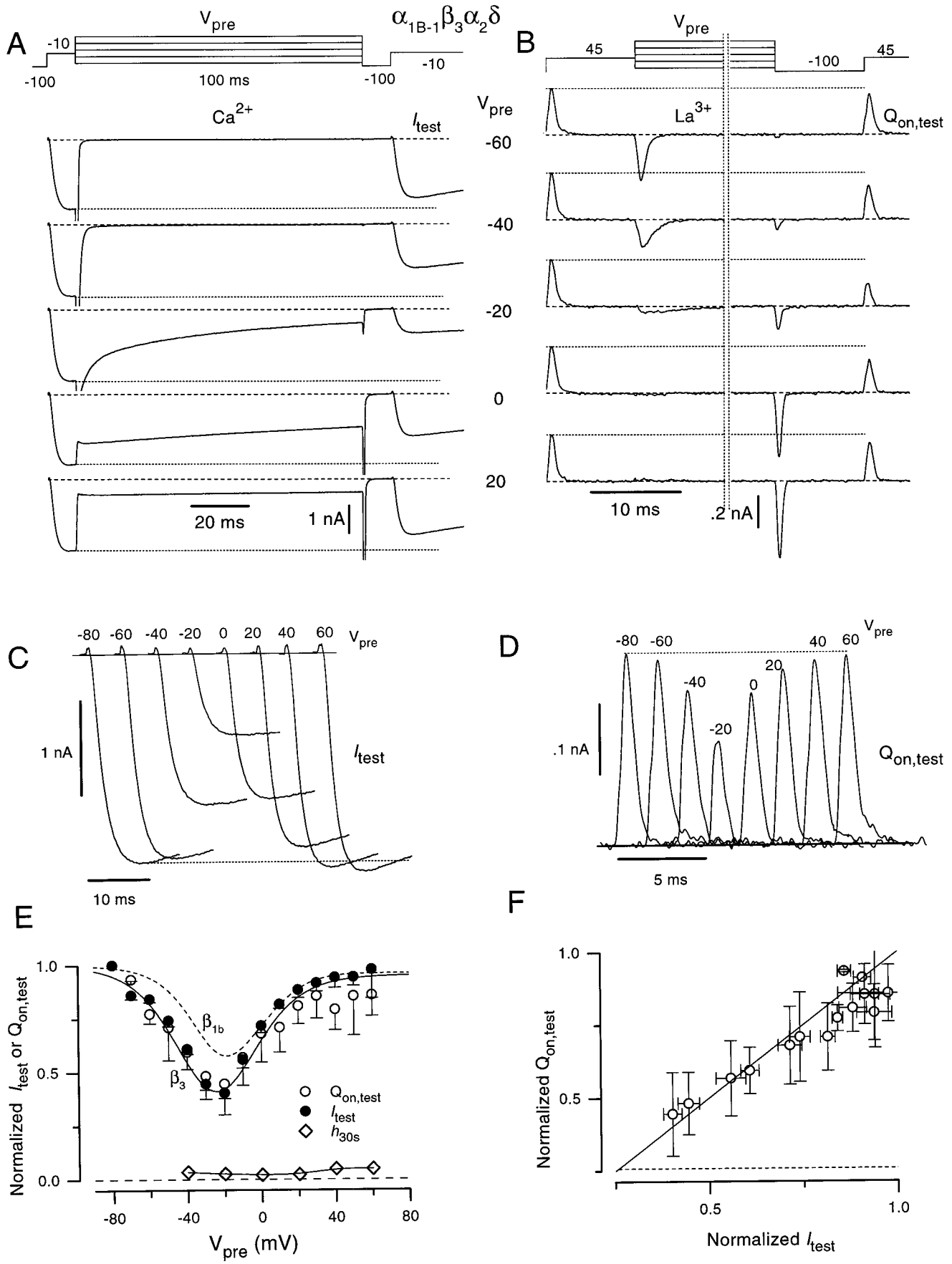
A
V_{pre}
$\alpha_{1B-1}\beta_3\alpha_2\delta$
-10
-100
100 ms
-100
-10
Ca^{2+}
I_{test}
V_{pre}
-60
-40
-20
0
20
20 ms
1 nA
B
V_{pre}
45
-100
45
La^{3+}
$Q_{on,test}$
10 ms
.2 nA
C
-80 -60 -40 -20 0 20 40 60 V_{pre}
1 nA
I_{test}
10 ms
D
-80 -60 40 60 V_{pre}
-40
0
20
-20
.1 nA
$Q_{on,test}$
5 ms
E
Normalized I_{test} or $Q_{on,test}$
1.0
0.5
0.0
β_{1b}
β_3
$Q_{on,test}$
I_{test}
h_{30s}
-80 -40 0 40 80
V_{pre} (mV)
F
Normalized $Q_{on,test}$
1.0
0.5
0.5 1.0
Normalized I_{test}

These events may underlie the slow component of "off" gating current, which returns the remainder of total charge. The right column of Fig. 10 *A* cartoons the Q-V relations that would result if one could separately measure gating currents from transitions among upper-row states (Q_A-V) or bottom-row states (Q_I-V), without contamination by interchange between rows. In practice, Q_I-V can only be approximated via kinetic separation of fast and slow components of gating current, as alluded to above. The smaller magnitude of the Q_I-V curve (Q_I) relative to the Q_A-V curve (Q_A = total gating charge) reflects restricted voltage-sensor movement by inactivation. In sodium channels, a similar form of "fast inactivation" involves the cytoplasmic III–IV linker (Vassilev et al., 1988; Stuhmer et al., 1989) according to a "hinged lid" mechanism (West et al., 1992). Similar gating charge effects (Armstrong and Bezanilla, 1977; Nonner, 1980; Armstrong, 1981) are seen with fast inactivation of sodium channels, and kinetic models resemble those for N-type inactivation (Armstrong, 1981; Stimers et al., 1985; Vandenberg and Bezanilla, 1991; but see Kuo and Bean, 1994).

"C-type" inactivation of potassium channels involves conformational changes at the external channel mouth (Fig. 10 *B*, *left*), which affects interactions with external Cd^{2+}, TEA, and sulfhydryl modifiers (Choi et al., 1991; Lopez-Barneo et al., 1993; Yellen et al., 1994; Baukrowitz and Yellen, 1995, 1996; Liu et al., 1996). Sensitivity to mutations in the carboxyl end of *Shaker* (S6 transmembrane region) gives rise to the term "C-type inactivation" (Hoshi et al., 1990). The state-diagram view (Fig. 10 *B*, *middle*) reflects coupling of activation and inactivation, because C-type inactivation also affects gating charge movement (Fedida et al., 1996; Olcese et al., 1997). However, by contrast to N-type inactivation, all of the gating charge is detected experimentally while channels remain C-type inactivated (Olcese et al., 1997), although such charge movement occurs only at negative potentials. These results argue for a full complement of I states and voltage-independent vertical transitions. Other results suggest that inactivation is increasingly favored with proximity to the open state (Olcese et al., 1997). Gating charge effects (Fig. 10 *B*, *right*) are represented by equimagnitude but widely separated Q_I-V and Q_A-V curves. The leftward shift of the Q_I-V produces observable gating charge immobilization by reducing charge moved over the normal activation range (V_A). Sodium channels exhibit a potentially related "slow inactivation" that is sensitive to mutations near or in the external channel mouth (Balser et al., 1996; Wang and Wang, 1997). Similar kinetic diagrams and gating charge effects pertain to slow inactivation of sodium channels (Bezanilla et al., 1982). L-type calcium channels manifest an analogous form of slow inactivation in skeletal muscle (Brum and Rios, 1987) and heart (Shirokov et al., 1993).

"P-type" inactivation of potassium channels, characterized by sensitivity to point mutation in the conduction pore, has also been reported (De Biasi et al., 1993). Mutation at the 469 position of a chimeric Kv2.1 channel with a Kv3.1 pore enhances P-type inactivation (De Biasi et al., 1993), and mutation at the 434 position of *Shaker* may also potentiate this inactivation (Yan et al., 1996). We exclude P-type inactivation in Fig. 10, because far less has been published about its physical features and gating charge effects. Nevertheless, the existence of P-type inactivation cautions against attributing all pore-related structural effects, or all non-N-type inactivation, to C-type inactivation or its potential correlates in other channels.

Comparison of N-type channel inactivation to prevailing forms of inactivation in potassium and sodium channels

How do the properties of N-type channel inactivation compare to those of N-type, C-type, or P-type inactivation? From the structural standpoint, there are interesting similarities to C-type inactivation, in that manipulation near the external face of N-type calcium channels affects inactivation. ω-Conotoxins are highly charged molecules (Olivera et al., 1994) that interact preferentially with inactivated N-type channels (Stocker et al., 1997). The selective toxin blockade of N-type channels when applied outside (McCleskey et al., 1987) but not inside cells (Feldman et al., 1987) suggests that inactivation is associated with externally detectable conformational rearrangement. Because ω-CTX-GVIA interacts particularly well with motifs I and III (Ellinor et al., 1994), which are believed to bracket the conduction pore, the inactivation-related conformational change could well be localized to the extracellular mouth of the channel, as in C-type inactivation. Depolarization-dependent antibody binding to a motif near the external mouth of structurally related P/Q-type calcium channels (Brice et al., 1997) could be another indication of large, inactivation-related structural changes in this region.

Fig. 11 illustrates the results of gating current experiments (analogous to protocols in Fig. 5 *A*) that provide supporting evidence for an action of ω-CTx-GVIA on N-type channel inactivation. Fig. 11 *A* compares an alignment of test pulse gating currents measured with simple La^{3+} blockade (*solid lines*) to gating currents measured in 2 mM Ca^{2+} with 2 μM ω-CTx-GVIA added (*dashed lines*). With

FIGURE 9 Prepulse effects on ionic currents (measured in 2 mM Ca^{2+}) and gating currents (recorded during La^{3+} blockade) for $\alpha_{1B\text{-}1}$ β_3 $\alpha_2\delta$ channels. The format is essentially identical to that in Fig. 8. (*A–D*) Data from cell 380_9. (*E*, *F*) 100-ms prepulse inactivation data averaged from the same (n = 3) cells. In *E*, "steady-state" inactivation data (*diamonds*) were averaged from separate (n = 5) *cells*, *with standard errors less than the symbol size*. *The voltage protocol for steady-state inactivation experiments was as in Fig*. 2 *A* (*top*), except that the prepulse duration was 30 s, and 60 s separated prepulse protocols. The bath contained 10 mM $BaCl_2$ added to the base external solution described in Materials and Methods.

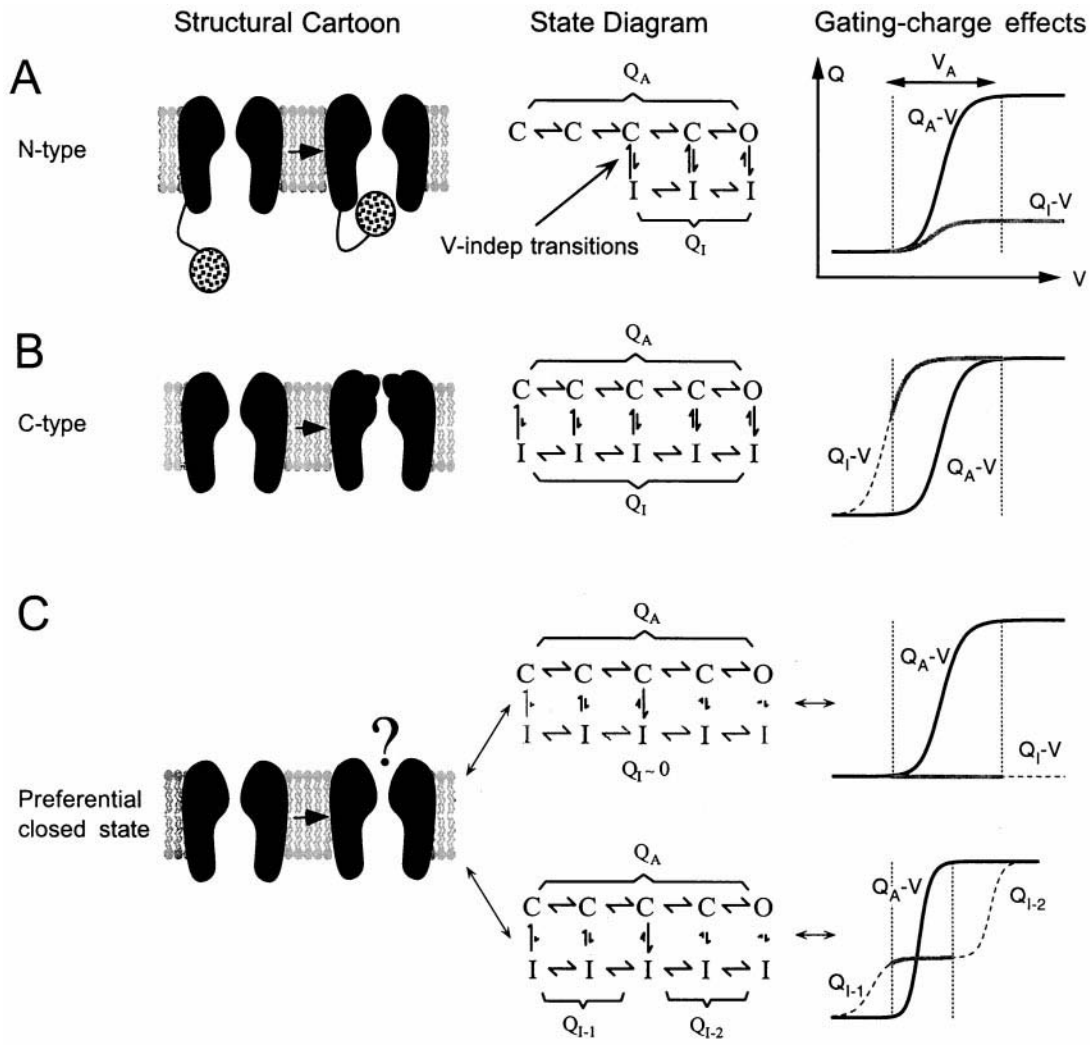

FIGURE 10 Models of voltage-dependent inactivation. (*A–C)* Each of the panels concerns a different inactivation mechanism, although all panels follow the same general format, as follows. On the left of each panel, we present a cartoon summarizing proposed structural rearrangements that underlie a particular inactivation mechanism. Conformations on the left and right correspond to noninactivated and inactivated channels. In the middle, the corresponding state diagram is shown. Here the diagram is intended to illustrate general features of a mechanism; the exact number of closed (C) and inactivated (I) states is not to be taken in a literal sense. The upper and lower rows of states correspond to voltage-dependent gating of noninactivated and inactivated channels, respectively. Q_A and Q_I indicate the amount of gating charge moved between the extremes of activated and inactivated states, respectively. Vertical transitions are voltage independent, with the possible exception of the upper kinetic scheme in *C*. Lengths of vertical transitions correspond symbolically to the relative sizes of the rate constants. On the right, we provide a qualitative depiction of the *Q-V* relations predicted for the corresponding inactivation mechanism. The voltage sensor movement of noninactivated channels corresponds to horizontal movement along the upper row of states (*middle column*) and gives rise to the solid black Q_A-*V* curve. Voltage sensor movement of inactivated channels corresponds to horizontal movement along the bottom row of states (*middle column*) and gives rise to the Q_I-*V* relation (*dashed and gray curve*). The dotted vertical lines indicate the voltage range (V_A) over which Q_A moves. The gray segments of Q_I-*V* curves indicate the portion of Q_I that moves over voltage range V_A; the vertical span of gray segments thus corresponds to the nonimmobilized charge. The dashed segments of Q_I-*V* curves indicate the portion of Q_I that moves outside V_A; the vertical span of dashed segments thus corresponds to immobilized gating charge. (*A*) "N-type" inactivation of potassium channels. The structural basis of this form of inactivation is a tethered intracellular ball that can plug the cytoplasmic mouth of an open channel. The maximum amplitude of the Q_I-*V* is reduced relative to the Q_A-*V*, because only a partial complement of inactivated states is present. The component of Q_I movement (*gray segment*) that occurs over V_A is diminished relative to the full magnitude of Q_A, giving rise to partial gating charge immobilization. (*B*) "C-type" inactivation of potassium channels. Conformational changes at the external mouth are believed to underlie this form of inactivation. A full complement of inactivated states (*bottom row*) is present, so that the maximum amplitudes of the Q_I-*V* and Q_A-*V* are identical. Inactivation is progressively favored with proximity to the "right" end of the gating scheme (*middle column*), resulting in a left shift of the Q_I-*V* (e.g., "charge 2" of Shirokov et al., 1992) relative to the Q_A-*V*. As with N-type inactivation (*A*), the component of Q_I movement (*gray segment*) that occurs over V_A is smaller than the full magnitude of Q_A, again giving rise to partial gating charge immobilization. (*C*) "Preferential closed-state inactivation" (PCSI) mechanisms proposed for N-type calcium channels. The structural basis of PCSI is largely unknown, although there are similarities to C-type inactivation (see text). Kinetic schemes underlying PCSI (*middle*) are distinguished by inactivation occurring most rapidly from intermediate closed states. Complete gating charge immobilization by inactivation can be accommodated by one of two general variations, which are not mutually exclusive. The first possibility (*middle*, *top*) is that I-I transitions are so slow that resulting gating currents would be undetectable. The exact number of I states is unspecified, although one I state situated under the middle of the activation pathway would suffice. These features are symbolized by the gray-tone representation of horizontal transitions among I states, as well as of unspecified I states. The choice of two gray-colored I states is arbitrary. The corresponding gating charge effect (*right*, *top*) is illustrated by a zero-amplitude Q_I-*V*,

ω-CTx-GVIA, a U-shaped dependence on prepulse voltage is still present but appears blunted relative to data measured during La^{3+} blockade. A comparison of average $Q_{on,test}$-V relations (Fig. 11 *B*) also reveals a large difference, thereby confirming the visual impression in Fig. 11 *A*. This perturbation of the charge movement supports enhancement of inactivation by ω-CTx-GVIA. Consistent with this premise, maximum gating charge declined slowly over the course of tens of minutes during exposure to ω-CTx-GVIA, as if channels continued to pool in stabilized inactivated states.

Another point of structural similarity to C-type inactivation is the locus of mutations and chimeric manipulations that influence calcium channel inactivation. Inactivation of structurally related R-type channels has important molecular determinants in IS6 (Zhang et al., 1994), and the inactivation of homologous P/Q-type channels is sensitively influenced by manipulations in IIIS5–IIIS6 (Tang et al., 1993) and IVS6 (Hering et al., 1996). All of these manipulations bear similarities to S6 mutations in *Shaker* potassium channels that influence C-type inactivation (Hoshi et al., 1991; Lopez-Barneo et al., 1993) and to external mouth mutations in sodium channels that alter slow inactivation (Balser et al., 1996; Wang and Wang, 1997).

However, two features of N-type channel inactivation contrast fundamentally with the expectations of either C-type or N-type inactivation of potassium channels. First, the reduction of mobile gating charge is directly proportional to the extent of ionic inactivation (Figs. 6 *D* and 3 *E*), with the implication that gating charge immobilization is complete in channels that are inactivated. This contrasts with N-type and C-type inactivation, both of which permit detectable charge movement over the normal activation range of the voltage sensor (range over which Q_I and Q_A movement overlaps, V_A in Fig. 10, *A* and *B*), resulting in the appearance of only partial gating charge immobilization. This suggests that the structural rearrangement underlying N-type channel inactivation is uniquely strong in the extent to which it restricts voltage sensor movement, in either a kinetic or an equilibrium sense.

Fig. 12 illustrates the second difference, which becomes apparent upon superposition of the prepulse inactivation curve for test pulse ionic current (I_{test}-V_{pre}, reproduced from Fig. 2 *B*), and the Q_{on}-V curve for gating currents (reproduced from Fig. 4 *F*). The nadir of the I_{test}-V_{pre} relation corresponds to a voltage at which the rate of inactivation is at maximum. The Q_{on}-V relation reports average channel position along the activation pathway as a function of voltage (Jones et al., 1997). The correlation between the two curves (*dotted lines*) indicates that only ~⅓ of voltage sensor activation has occurred by voltages at which the inactivation rate is at maximum. By contrast, N-type and C-type inactivation of potassium channels would exhibit a maximum inactivation rate upon full activation of voltage sensors (see Fig. 10, *A* and *B*). The unusual correlation in Fig. 12 *A* intuitively suggests that inactivation occurs most rapidly from closed states at intermediate positions along

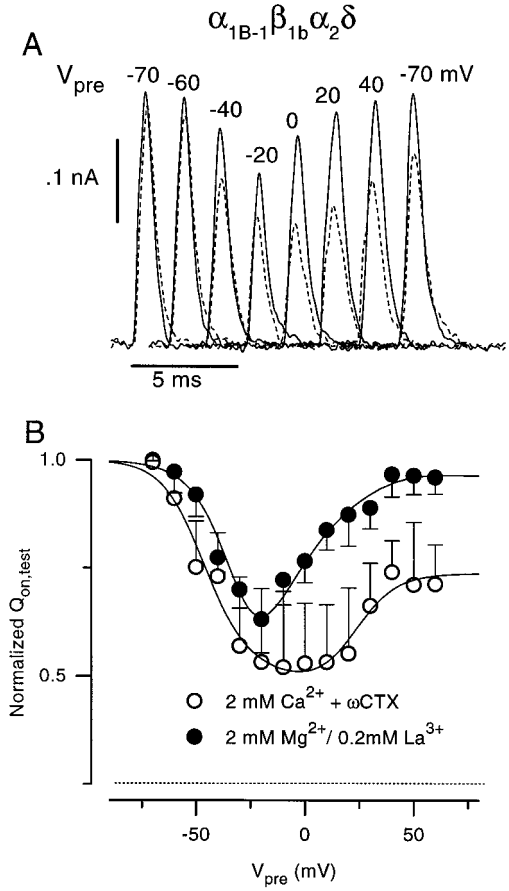

FIGURE 11 Effect of ω-conotoxin GVIA on prepulse inactivation of α_{1B-1} β_{1b} $\alpha_2\delta$ channels. (*A*) Comparison of aligned test pulse gating currents (format analogous to that in Fig. 6 *B*) measured either during blockade with La^{3+} (*solid lines*) or with 2 μM ω-conotoxin GVIA (2 mM Ca^{2+} present, *dashed lines*). All data are from cell 351_1, transfected with α_{1B-1} β_{1b} $\alpha_2\delta$. Note that the rightmost trace, which corresponds to V_{pre} = −70 mV, was acquired after all of the others. Comparison to the leftmost (earliest) trace, which also corresponds to V_{pre} = −70 mV, illustrates the slow decline of gating current that occurred in the presence of ω-CTX. This decline is consistent with gradual pooling of channels in inactivated states that were stabilized by the toxin. (*B*) Comparison of averaged $Q_{on,test}$-V_{pre} relations obtained with either block by La^{3+} (*closed circles*) or block by ω-CTX (*open circles*) for the same four cells.

equivalent to complete gating charge immobilization. The second possible kinetic scheme (*middle*, *bottom*) is similar to that for C-type inactivation, in that a full complement of I states is present and vertical transitions are voltage insensitive. Here, however, inactivation stabilizes an intermediate position of the voltage sensor. Consequently, the Q_I-V (*right*, *bottom*) is split into a negatively shifted component (Q_{I-1} analogous to "charge 2"), and a positively shifted component (Q_{I-2}). In contrast to N-type and C-type inactivation mechanisms (*A*, *B*), there is essentially no Q_I movement over the voltage range V_A, as shown graphically by the flatness of the gray Q_I-V region. Consequently, inactivation would result in complete gating charge immobilization over the voltage range used in this study.

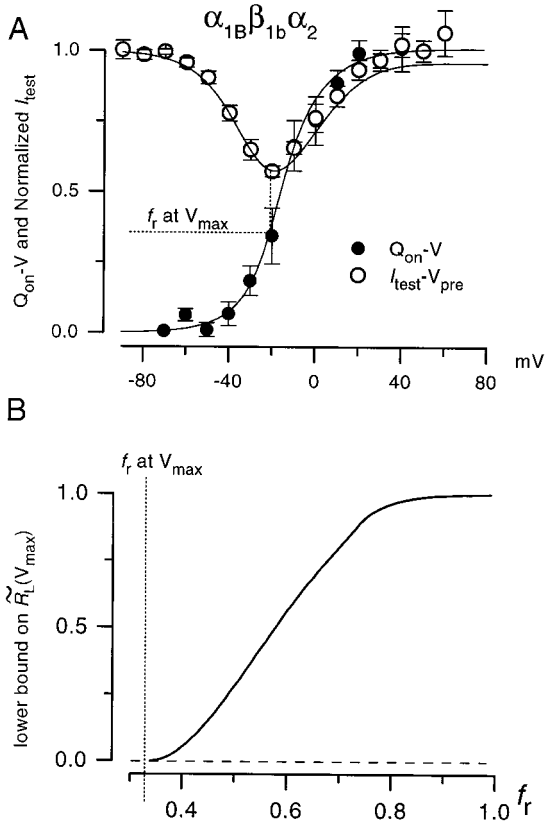

FIGURE 12 (*A*) Comparison of the voltage dependence of ionic current inactivation (*open circle*, I_{test}-V_{pre}, reproduced from Fig. 2 *B*) and gating charge movement (*closed circle*, Q_{on}-*V*, reproduced from Fig. 4 *F*), for cells transfected with $\alpha_{1B\text{-}1}\ \beta_{1b}\ \alpha_2\delta$. Dotted lines illustrate the fraction of gating charge moved ($\sim$⅓) when the rate of ionic current inactivation is at maximum ($V_{pre} \approx -20$ mV). (*B*) Lower bound for the fraction of the maximum inactivation rate owing to inactivation from a "left" group of closed states (given by $\tilde{R}_L(V_{max})$ in Eq. A15, Appendix). The maximum inactivation rate of the channel is that observed at voltage $V_{max} \approx -20$ mV, at the nadir of the prepulse inactivation curve (*A*). Closed states in the "left" group are defined as those that correspond to fractional voltage-sensor positions less than f_r. The graph plots the lower limit for $\tilde{R}_L(V_{max})$ as a function of f_r.

the activation pathway (e.g., Fig. 10 *C*, *center*). Analytic arguments confirm this intuitive proposal, as summarized below. Details of the analysis are presented in the Appendix.

From consideration of the partition function that describes equilibrium probabilities of states S_i in the normal activation pathway (Sigg and Bezanilla, 1997), we can use experimentally measured *Q*-*V* and prepulse inactivation curves to calculate a lower limit on the amount of inactivation that must occur from states located to the "left" of an arbitrary boundary in the normal activation pathway. These analytical considerations will ultimately lead us to conclude that at the voltage V_{max} (i.e., at the minimum of the prepulse inactivation curve), where the channel inactivates most rapidly, essentially all of the inactivation occurs from closed conformations that are "far" from the open state. Specifically, we define the "position" of a state S_i in the activation pathway by the amount of gating charge q_i that is moved as a channel transitions from the deepest (*leftmost* in Fig. 10) closed state to S_i. In practice, we specify state position in terms of the "fractional position of the voltage sensor" ($f_i = q_i/Q_{max}$) when the channel resides in state S_i. States in the "left half" of the activation pathway can then be identified by a fractional position f_i that is less than an arbitrary boundary value of f_r. Given these definitions, we can calculate a lower limit for $\tilde{R}_L(V_{max})$, where $\tilde{R}_L(V_{max})$ quantifies the net inactivation from all states in the "left" group, expressed as a fractional contribution to the maximum inactivation rate at V_{max}. Equation A15 (Appendix) gives the explicit formula for a lower limit on $\tilde{R}_L(V_{max})$, which turns out to be a function of f_r, the normalized *Q*-*V* (e.g., Fig. 4 *F*), the normalized prepulse inactivation curve (e.g., Fig. 2 *B*), and the total gating charge per calcium channel (Q_{max}, taken to be 16 e_o, from Noceti et al. (1996)). Fig. 12 *B* plots the lower limit for $\tilde{R}_L(V_{max})$, here calculated for $\alpha_{1B\text{-}1}\ \beta_{1b}\ \alpha_2\delta$ channels. The striking feature of this lower limit is that it essentially reaches unity by $f_r = 0.8$. In other words, when the channel is inactivating at the fastest possible rate, virtually all of the inactivation is coming from closed conformations corresponding to fractional voltage sensor positions of less that 0.8 (i.e., from states at a substantial "distance" from the open state). This analysis strongly supports mechanisms in which inactivation occurs preferentially from intermediate closed states along the activation pathway. It is worth emphasizing that the lower limit in Fig. 12 *B* is by no means the strongest bound in favor of closed-state inactivation, but, quite remarkably, it is a constraint that emerges from essentially analytic grounds, given the correlation between the *Q*-*V* and the prepulse inactivation curves in Fig. 12 *A*. In this regard, the constraint is quite general because it does not depend on the choice of a particular kinetic scheme.

Preferential closed-state inactivation of recombinant N-type calcium channels

The distinctive properties of N-type channel inactivation argue in favor of "preferential closed-state inactivation" (PCSI) mechanisms, which have also recently been proposed for inactivation of Kv2.1 potassium channels (Klemic et al., 1998). Fig. 10 *C* summarizes the key properties of PCSI for recombinant N-type calcium channels. The structure-function basis of PCSI remains an open frontier (Fig. 10 *C*, *left*), although there are intriguing hints that PCSI shares structural similarities with C-type inactivation (modulation of inactivation by blockade of the external mouth, sensitivity to pore and S6 mutations, as elaborated above).

Regarding kinetic state diagrams (Fig. 10 *C*, *center*, *either top or bottom layout*), a number of specific constraints emerge from the experiments. First, PCSI mechanisms are distinguished by schemes in which the most rapid (C, O) $\rightarrow$ I transitions emanate from intermediate closed conformations along the activation pathway. This feature contrasts with customary formulations of N- or C-type inactivation

(Fig. 10, *A* and *B*), in which transitions to I states are most rapid from conformations near the open state.

Second, to account for nearly complete steady-state inactivation at depolarized potentials (Fig. 9 *E*), (C, O) ↔ I transitions near the open conformation must favor inactivated states at equilibrium. If (C, O) ↔ I transitions are largely voltage independent, as found with N- and C-type inactivation, then this constraint would hold true at all potentials; otherwise, the constraint must at least hold at depolarized potentials. These constraints presume that steady-state inactivation (Fig. 9 *E*) reflects the same inactivation process that predominates during shorter 100-ms prepulses.

Finally, either of two additional features is required by the complete immobilization of measurable gating charge by inactivation. These features are not mutually exclusive. The top diagram in Fig. 10 *C* (*center*) represents one possibility. Here, the movement among inactivated states occurs too slowly to produce measurable gating current, although such movement may occur on a longer time scale. Gating charge immobilization thus arises from the lack of measurable movement among voltage-dependent I-I transitions. No commitment is made as to the number of I states, and the existence of only a single I state would suffice as a specific case example. Gating charge effects of this first scenario are therefore diagrammed with a flat Q_I-V curve (Fig. 10 *C*, *top right*), signifying the lack of measurable gating current arising from I-I transitions.

The bottom diagram in Fig. 10 *C* (*center*) illustrates the second possible explanation for complete gating charge immobilization by inactivation. Here, in similarity to C-type inactivation, measurable gating charge movement can arise from redistribution among a full complement of inactivated states, and (C, O) ↔ I transitions are largely voltage independent. However, in the case of PCSI, the voltages where such gating charge movement can be detected are far more removed from the activation range (V_A) than observed with C-type inactivation. Consequent to considerations of microscopic reversibility and the constraint that fastest inactivation occurs from mid-closed states, steady-state Q_I-V curves could manifest a wide and flat plateau that separates hyperpolarized $Q_{I\text{-}1}$ and depolarized $Q_{I\text{-}2}$ phases. The appearance of complete gating charge immobilization with inactivation could therefore arise because our study may have been limited to voltages spanning the flat plateau region. However, gating currents arising from I-I transitions might still be detected at extreme voltages where $Q_{I\text{-}1}$ and $Q_{I\text{-}2}$ phases occur. This is an interesting possibility that could be tested in future studies, if the requisite voltages turn out to be experimentally feasible.

Most of the N-type channel results can also be explained by an alternative, voltage-dependent inactivation mechanism in which the transition from a single inactivated state to the open state is voltage dependent and favored at depolarized potentials (Jones and Marks, 1989). This model provides a natural explanation for gating charge immobilization and U-shaped inactivation. However, this model does not account for essentially complete steady-state inactivation with increasing depolarization, as observed in Fig. 9 *E*.

Generalizability of preferential closed-state inactivation to native N-type channels

Native N-type channels in sympathetic neurons share several core properties (Jones and Marks, 1989) that support a preferential closed-state inactivation model. Prepulse inactivation is U-shaped with respect to voltage; the rate of inactivation is essentially unchanged with different concentrations of Ba^{2+} and Ca^{2+} as charge carrier; and there are small effects of increased intracellular Ca^{2+} buffering. It is therefore reasonable to expect that our results will generalize to native N-type channels in a number of settings.

On the other hand, there are indications that N-type channels in chick dorsal root ganglion (DRG) neurons may be inactivated, at least in part, by a strong current-dependent mechanism (Kasai and Aosaki, 1988; Cox and Dunlap, 1994). Here, prepulse inactivation is again U-shaped and similar with Ba^{2+} or Ca^{2+} as the charge carrier. However, inactivation of Ba^{2+} or Ca^{2+} currents is blunted by increased intracellular buffering of divalent cations. In addition, inactivation is markedly slowed when Na^+ flows through these N-type channels, as can be seen in the virtual absence of divalent cations (Morad et al., 1988; Cox and Dunlap, 1994).

Taken at face value, these results argue that the inflow of divalent cations speeds inactivation. Given this interpretation, it could be that different splice variants of N-type channels differ with regard to their inactivation properties; those in chick DRG neurons (Kasai and Aosaki, 1988; Cox and Dunlap, 1994) would inactivate in a partially current-dependent fashion, whereas those in frog sympathetic neurons (Jones and Marks, 1989) and human $\alpha_{1B\text{-}1}$ expressed in HEK 293 cells (this study) would inactivate in a largely or purely voltage-dependent manner.

Alternatively, the buffering and monovalent current data could be interpreted within the framework of purely voltage-dependent inactivation. Increased intracellular buffering of Ca^{2+} could alter basal protein kinase C activity or G-protein activation, which in turn could result in modulation of a fundamentally voltage-dependent inactivation mechanism (Werz et al., 1993). The strict withdrawal of divalent cations, which permits monovalent flux through N-type channels, may strip the channel of divalent cations that are required for proper function, resulting in an artifactual slowing of inactivation. Such a proposal has precedent in *Shaker* potassium channels, where withdrawal of divalent cations causes channels to "debase" and manifest altered properties of gating and selectivity (Armstrong and Miller, 1990). Although there is no clear evidence for such altered gating in calcium channels, it is interesting to note that monovalent cation currents through L-type calcium channels inactivate slowly in the strict absence of divalent cations, but upon addition of trace (20 μM) Ca^{2+}, monovalent

currents inactivate just as rapidly as seen with millimolar Ba^{2+} as the charge carrier (Ferreira et al., 1997). Such trace external Ca^{2+} should be insufficient (Lansman et al., 1986) to populate a binding site for current-dependent inactivation, which must have a relatively low affinity to explain the variation of inactivation rate in the presence of millimolar concentrations of calcium. However, trace Ca^{2+} could bind to a high-affinity site that induces proper operation of voltage inactivation. If this alternative set of interpretations holds true, then inactivation of N-type channels in chick DRG neurons could be essentially the same as observed here for the human N-type channel.

These considerations indicate that a voltage-dependent, preferential closed-state inactivation mechanism may also apply to a number of native N-type channels. However, universal applicability of this mechanism must await resolution of some of the ambiguities outlined above.

CONCLUSION

This study and that of Patil et al. (1998) establish a functional roadmap of N-type channel inactivation, as manifested by human N-type channels expressed in HEK 293 cells. The inactivation of these channels has important implications for calcium channel inactivation during trains of action potentials (Borst et al., 1997; Forsythe et al., 1998) and has several unusual features. First, prepulse inactivation bears a U-shaped dependence on voltage, yet the inactivation appears to be entirely voltage dependent, based on the gating current data presented here and altered charge carrier and buffering experiments performed by Patil et al. (1998). Second, the gating charge immobilization produced by inactivation is more complete than observed in most other channels. Third, the interrelation between prepulse inactivation and *Q-V* relations (Fig. 12) provides new and strong evidence that channels inactivate most rapidly from intermediate closed states along the activation pathway, as initially suggested by our laboratory on the basis of ionic current experiments alone (Patil et al., 1998). Despite these distinctive features, mutagenesis (Tang et al., 1993; Zhang et al., 1994; Hering et al., 1996) and toxin experiments (Stocker et al., 1997, and Fig. 11) hint that structural rearrangements at the external mouth of the channel may underlie N-type channel inactivation, as would be expected for a mechanism related to C-type inactivation. It will be interesting to see if further structural correlates to this inactivation offer insight into the unusual functional properties of N-type channel inactivation.

APPENDIX

Here we develop analytic arguments that demonstrate how the experimentally measured prepulse inactivation and *Q-V* relations exert substantial constraints in favor of preferential closed-state inactivation. The main outcome of the analysis is summarized in the text and in Fig. 12 *B*. The detailed deductions follow.

Definitions

S_i = the ith state in the activation pathway, where i is an integer.

q_i = gating charge moved as a channel transitions to the state S_i from the most favored state(s) at infinite hyperpolarization.

Q_{max} = total gating charge of all of the voltage sensors in a channel.

$f_i = q_i/Q_{max}$ = fractional position of the voltage sensor (in "normalized gating charge movement coordinates") when a channel occupies state S_i. Given this definition, we also define that $j > i$ means $f_j > f_i$. In a typical linear activation scheme ($C \rightleftharpoons C \cdots C \rightleftharpoons O$), S_j would be "farther to the right" along the activation pathway than S_i.

k_i = rate constant of inactivation from state S_i.

$P_i(V)$ = probability of occupying state S_i at equilibrium, given that a channel is not inactivated. This probability is related to the free-energy profile of the various states in the activation pathway by

$$P_i(V) = \frac{\exp(-F_i/kT)}{\sum_m(\exp(-F_m/kT))} \tag{A1}$$

which is the partition function for $P_i(V)$ (see Sigg and Benzanilla, 1997). Here, $F_i = g_i - q_iV$, where g_i is the chemical free energy of a channel in state S_i, and the summation on m spans all noninactivated states.

$Q(V) = \Sigma_i q_i P_i(V)$ = the steady-state voltage dependence of gating-charge movement.

$\tilde{Q}(V) = Q(V)/Q_{max}$ = normalized $Q(V)$ relation. This predicts the experimentally measured "*Q-V*" relations.

$R(V) = \Sigma_i k_i P_i(V)$ = rate of inactivation of a noninactivated channel. V_{max} is the voltage at which $R(V)$ is maximized. We refer to the maximum inactivation rate as R_{max}.

$\tilde{R}(V) = R(V)/R_{max}$ = normalized $R(V)$ relation.

Assumptions

To obtain calculable constraints that favor closed-state inactivation, we will link the analytic entity $R(V) = \Sigma_i k_i P_i(V)$ to experimentally measured prepulse inactivation data (e.g., normalized I_{test} in Fig. 2 *B*). We adopt the approximation that

$$\tilde{R}(V) = \frac{R(V)}{R_{max}} \approx \frac{\ln(\text{normalized } I_{test}(V))}{\ln(\text{normalized } I_{test}(V_{max}))} \tag{A2}$$

This approximation makes two assumptions. First, noninactivated channels are in rapid equilibrium along the activation pathway, relative to the characteristic rate of inactivation. This is reasonable, because activation and deactivation are rapid events relative to both the typical rate of inactivation and the 100-ms duration of the prepulse. Second, channels do not return from inactivation during a 100-ms prepulse. This condition seems reasonable, because prepulse inactivation occurs primarily at voltages where steady-state inactivation is essentially complete, as demonstrated by the near-zero values of the steady-state inactivation curve over the relevant voltage range (Fig. 9 *E*, *diamonds*). If the essentially complete steady-state inactivation reflects the same process that dominates during shorter 100-ms prepulses, then returns from inactivation must be exceedingly rare during a 100-ms prepulse, as we assume. Given these two assumptions, we can write the following differential equation that describes the time-dependent change of $A(t)$, the fraction of noninactivated channels at time t in the prepulse

$$\frac{dA}{dt} = -\underbrace{\left(\sum_i k_i P_i(V)\right)}_{R(V)} A$$

This yields the result that

$$\text{normalized } I_{test}(V) = A(T) = \exp(-R(V)T)$$

where T is the 100-ms duration of the prepulse. Taking the natural logarithm of both sides yields

$$R(V) = -\frac{\ln(\text{normalized } I_{\text{test}}(V))}{T}$$

This expression can be used to calculate the approximation in Eq. A2.

Calculation of the voltage at which $P_i(V)$ is maximum

The maximum of $P_i(V)$ will be found at the voltage $V_{max,i}$ where $dP_i(V)/dV = 0$. Evaluating this derivative reveals a remarkably simple relation between the Q-V curve and $V_{max,i}$. This is an important result that will prove useful in the deductions below and in the Discussion. From Eq. A1, we have

$$\frac{dP_i}{dV} = \frac{\exp(-F_i/kT)}{\sum_m(\exp(-F_m/kT))}\left[\frac{q_i}{kT} - \sum_n\left(\frac{q_n}{kT}\frac{\exp(-F_n/kT)}{\sum_p(\exp(-F_p/kT))}\right)\right] \quad \text{(A3)}$$

Simplifying Eq. A3 with Eq. A1 yields

$$\frac{dP_i}{dV} = \frac{P_i(V)}{kT}[q_i - Q(V)] \quad \text{(A4)}$$

Setting the derivative to zero, we conclude that $P_i(V)$ reaches a maximum at the voltage $V_{max,i}$ where $q_i = Q(V)$. In terms of normalized relations,

$$f_i = \tilde{Q}(V_{max,i}) \quad \text{(A5)}$$

In other words, $P_i(V)$ reaches a maximum at the voltage $V_{max,i}$ where the $\tilde{Q}(V)$ curve intersects a horizontal line at value f_i.

Derivation of $P_i(V)$ as a function of $\tilde{Q}(V)$, f_i, Q_{max}, and the value of $P_i(V)$ at a single arbitrary voltage V_o

From Eq. A4, we can write

$$\frac{d\ln(P_i)}{dV} = \frac{1}{kT}(q_i - Q(V))$$

Integrating with respect to voltage from V_o to V yields

$$\frac{P_i(V)}{P_i(V_o)} = \exp\left(\frac{Q_{max}}{kT}\left[f_i(V - V_o) - \int_{\sigma=V_o}^{\sigma=V}\tilde{Q}(\sigma)d\sigma\right]\right) \quad \text{(A6)}$$

Note that the form of this function is determined solely by f_i, $\tilde{Q}(V)$, and Q_{max}. For notational clarity in subsequent sections, we define

$$h_i(V, V_o) = \exp\left(\frac{Q_{max}}{kT}\left[f_i(V - V_o) - \int_{\sigma=V_o}^{\sigma=V}\tilde{Q}(\sigma)d\sigma\right]\right) \quad \text{(A7)}$$

Upper bound on net inactivation from states with $f \geq f_r$

We can use the relation for the voltage dependence of the $P_i(V)$ (Eq. A6) to derive an upper bound on the net inactivation rate from all states with fractional position $f \geq f_r$, where state S_r has the smallest gating charge movement q_r within this group of states. In the context of a linear activation scheme, we are thus deriving an upper bound for net inactivation from state S_r and all states to the "right" of it—hence the subscript r for the "border" state S_r. Likewise, we define these states as members of group D (for *dextro*, or toward the right). The remainder of states to the "left" of S_r are members of group L (for *left* group of states). An important feature of the upper bound to be established is that it is calculable from experimentally measured parameters.

We can obtain the desired bound by considering the defining relation for inactivation rate for states in group D ($R_D(V) = \Sigma_{i\in D}k_iP_i(V)$, written by analogy to the form of $R(V)$ given in the definitions). Substituting from Eqs. A6 and A7, and setting the reference voltage $V_o = V_{max,r}$, where $V_{max,r}$ maximizes occupancy in state S_r, we obtain

$$R_D(V) = \sum_{i\in D} k_iP_i(V_{max,r})h_i(V, V_{max,r}) \quad \text{(A8)}$$

To derive an upper bound on $R_D(V)$, we first establish an upper bound on $h_i(V, V_{max,r})$ with $i \in D$. We can obtain the latter bound by considering the ratio of $h_i(V, V_{max,r})$ to $h_r(V, V_{max,r})$ with $i \in D$. From Eq. A7, we have

$$\frac{h_i(V, V_{max,r})}{h_r(V, V_{max,r})} = \exp\left(\frac{Q_{max}}{kT}(f_i - f_r)(V - V_{max,r})\right) \quad \text{(A9)}$$

For $V < V_{max,r}$, the argument of the exp function is negative, except when $i = r$, where it is zero. Hence, $h_i(V, V_{max,r}) \leq h_r(V, V_{max,r})$, for $i \in D$ and $V < V_{max,r}$. With this bound on $h_i(V, V_{max,r})$, we can convert Eq. A8 into an upper bound on $R_D(V)$:

$$R_D(V) \leq h_r(V, V_{max,r})\sum_{i\in D} k_iP_i(V_{max,r}) \quad \text{(A10)}$$

for $i \in D$ and $V < V_{max,r}$. The only problem with this upper bound is that we have no experimental measure of the summation term, which is equal to $R_D(V_{max,r})$, the net inactivation rate from D group states at voltage $V_{max,r}$. On the other hand, the other term, $h_r(V, V_{max,r})$, can be calculated from experimentally measured parameters. To address this deficiency, we consider another upper bound on $R_D(V)$ that, although less stringent, can be determined from experimental data. Because the summation term in Eq. A10 ($=R_D(V_{max,r})$) is certainly less than or equal to the net inactivation rate from all states at voltage $V_{max,r}$ ($=R(V_{max,r})$), we can substitute $R(V_{max,r})$ for the summation term to obtain

$$R_D(V) \leq h_r(V, V_{max,r})R(V_{max,r}) \quad \text{(A11)}$$

for $i \in D$ and $V < V_{max,r}$. Dividing through by the maximum inactivation rate R_{max} yields the more convenient, normalized version of this constraint:

$$\tilde{R}_D(V) = \frac{R_D(V)}{R_{max}} \leq h_r(V, V_{max,r})\frac{R(V_{max,r})}{R_{max}} = h_r(V, V_{max,r})\tilde{R}(V_{max,r}) \quad \text{(A12)}$$

for $i \in D$ and $V < V_{max,r}$. Substituting $\tilde{R}(V_{max,r}) \approx \ln(\text{normalized } I_{test}(V_{max,r}))/\ln(\text{normalized } I_{test}(V_{max}))$ (from the Assumptions, above) into Eq. A12 and expressing $h_r(V, V_{max,r})$ explicitly as given in Eq. A7 yields the experimentally calculable constraint

$$\tilde{R}_D(V) \leq \exp\left(\frac{Q_{max}}{kT}\left[f_r(V - V_{max,r}) - \int_{\sigma=V_{max,r}}^{\sigma=V} Q(\sigma)d\sigma\right]\right) \times \frac{\ln(\text{normalized } I_{test}(V_{max,r}))}{\ln(\text{normalized } I_{test}(V_{max}))} \quad \text{(A13)}$$

for $i \in D$ and $V < V_{max,r}$. The terms in the argument of the exp function can be calculated from our Q-V curves and from estimates of Q_{max} by Noceti et al. (1996). As well, the normalized I_{test} term can be derived from prepulse inactivation data. Hence, although Eq. A13 is not the strongest

upper bound on $\tilde{R}_D(V)$, it is one that we can calculate from experimental data.

Lower bound on net inactivation from states with $f < f_r$

For purposes of establishing an experimentally determined constraint in favor of closed-state inactivation, it is perhaps more convenient to calculate a lower bound on net inactivation from L group states to the "left" of S_r, i.e., those states with $f < f_r$. This bound is easy to formulate from the already established upper bound on $\tilde{R}_D(V)$. It is evident that

$$\tilde{R}_L(V) = \tilde{R}(V) - \tilde{R}_D(V)$$

If we choose $V = V_{max}$, the voltage at which the overall inactivation rate from all states is at maximum, then the above expression simplifies to

$$\tilde{R}_L(V_{max}) = 1 - \tilde{R}_D(V_{max}) \tag{A14}$$

Substituting the upper bound for $\tilde{R}_D(V_{max})$ from Eq. A13 into Eq. A14 yields the lower bound for $\tilde{R}_L(V_{max})$:

$$\tilde{R}_L(V_{max}) \geq 1 - \exp\left(\frac{Q_{max}}{kT}\left[f_r(V_{max} - V_{max,r}) - \int_{\sigma=V_{max,r}}^{\sigma=V_{max}} \tilde{Q}(\sigma)\mathrm{d}\sigma\right]\right) \times \frac{\ln(\text{normalized } I_{test}(V_{max,r}))}{\ln(\text{normalized } I_{test}(V_{max}))} \tag{A15}$$

for $i \in D$ and $V_{max} < V_{max,r}$. These conditions will be met if $f_r \geq \tilde{Q}(V_{max})$, because $f_r = \tilde{Q}(V_{max,r})$, and $\tilde{Q}$ is a monotonically rising function of voltage. Equation A15 is plotted in Fig. 12 *B* to establish a minimal constraint in favor of preferential closed-state inactivation. Although this bound is not necessarily the best lower bound, it is derivable from experimental measures.

We thank SIBIA Neurosciences for the $\alpha_{1B\text{-}1}$ clone, T. P. Snutch for the $\alpha_2\delta$ clone, K. P. Campbell for the β_{1b} clone, and E. Perez-Reyes for the β_{2a} and β_3 clones. We are also grateful to Parag Patil, Henry Colecraft, and Pancho Bezanilla for discussion and comments, and to J. G. Mulle and R. Zhang for technical assistance.

This work was supported by the National Institutes of Health (RO1 to DTY, Medical Scientist Training Program Award to LPJ).

REFERENCES

Aldrich, R. W. 1981. Inactivation of voltage-gated delayed potassium current in molluscan neurons. A kinetic model. *Biophys. J.* 36:519–532.

Armstrong, C. M. 1981. Sodium channels and gating currents. *Physiol. Rev.* 61:644–683.

Armstrong, C. M., and F. Bezanilla. 1977. Inactivation of the sodium channel. II. Gating current experiments. *J. Gen. Physiol.* 70:567–590.

Armstrong, C. M., and C. Miller. 1990. Do voltage-dependent K^+ channels require Ca^{2+}? A critical test employing a heterologous expression system. *Proc. Natl. Acad. Sci. USA.* 87:7579–7582.

Balser, J. R., H. B. Nuss, N. Chiamvimonvat, M. T. Perez-Garcia, E. Marban, and G. Tomaselli. 1996. External pore residue mediates slow inactivation in μl rat skeletal sodium channels. *J. Physiol. (Lond.).* 494:431–442.

Baukrowitz, T., and G. Yellen. 1995. Modulation of K^+ current by frequency and external $[K^+]$: a tale of two inactivation mechanisms. *Neuron.* 15:951–960.

Baukrowitz, T., and G. Yellen. 1996. Use-dependent blockers and exit rate of the last ion from the multi-ion pore of a K^+ channel. *Science.* 271:653–656.

Bean, B. P. 1989. Neurotransmitter inhibition of neuronal calcium currents by changes in channel voltage dependence. *Nature.* 340:153–156.

Bean, B. P., and E. Rios. 1989. Nonlinear charge movement in mammalian cardiac ventricular cells. Components from Na and Ca channel gating. *J. Gen. Physiol.* 94:65–93.

Bezanilla, F. 1985. Gating of sodium and potassium channels. *J. Membr. Biol.* 88:97–111.

Bezanilla, F., E. Perozo, D. M. Papazian, and E. Stefani. 1991. Molecular basis of gating charge immobilization in Shaker potassium channels. *Science.* 254:679–683.

Bezanilla, F., and E. Stefani. 1994. Voltage-dependent gating of ionic channels. *Annu. Rev. Biophys. Biomol. Struct.* 23:819–846.

Benzanilla, F., R. Taylor, and J. Fernandez. 1982. Distribution and kinetics of membrane dielectric polarization. I. Long-term inactivation of gating currents. *J. Gen. Physiol.* 79:21–40.

Borst, J. G., F. Helmchen, and B. Sakmann. 1997. A decrease in presynaptic calcium influx may contribute to synaptic depression (abstract). *J. Gen. Physiol.* 110:18a.

Brehm, P., and R. Eckert. 1978. Calcium entry leads to inactivation of calcium channel in *Paramecium. Science.* 202:1203–1206.

Brice, N. L., N. S. Berrow, V. Campbell, K. M. Page, K. Brickley, I. Tedder, and A. C. Dolphin. 1997. Importance of the different beta subunits in the membrane expression of the alpha-1A and alpha-2 calcium channel subunits—studies using a depolarization-sensitive alpha-1A antibody. *Eur. J. Neurosci.* 9:749–759.

Brum, G., and E. Rios. 1987. Intramembrane charge movement in frog skeletal muscle fibres. Properties of charge 2. *J. Physiol. (Lond.).* 387: 489–517.

Castellano, A., X. Wei, L. Birnbaumer, and E. Perez-Reyes. 1993. Cloning and expression of a third calcium channel beta subunit. *J. Biol. Chem.* 268:3450–3455.

Choi, K. L., R. W. Aldrich, and G. Yellen. 1991. Tetraethylammonium blockade distinguishes two inactivation mechanisms in voltage-activated K^+ channels. *Proc. Natl. Acad. Sci. USA.* 88:5092–5095.

Cox, D. H., and K. Dunlap. 1994. Inactivation of N-type calcium current in chick sensory neurons: calcium and voltage dependence. *J. Gen. Physiol.* 104:311–336.

De Biasi, M., H. A. Hartmann, J. A. Drewe, M. Taglialatela, A. M. Brown, and G. E. Kirsh. 1993. Inactivation determined by a single site in K^+ channels. *Pflügers Arch.* 422:354–363.

Demo, S. D., and G. Yellen. 1991. The inactivation gate of the *Shaker* K^+ channel behaves like an open-channel blocker. *Neuron.* 7:743–753.

Dubel, S. J., T. V. Starr, J. Hell, M. K. Ahlijanian, J. J. Enyeart, W. A. Catterall, and T. P. Snutch. 1992. Molecular cloning of the alpha-1 subunit of an omega-conotoxin-sensitive calcium channel. *Proc. Natl. Acad. Sci. USA.* 89:5058–5062.

Dunlap, K., J. I. Luebke, and T. J. Turner. 1995. Exocytotic Ca^{2+} channels in mammalian central neurons. *Trends Neurosci.* 18:89–98.

Eckert, R., and J. E. Chad. 1984. Inactivation of Ca channels. *Prog. Biophys. Mol. Biol.* 44:215–267.

Ellinor, P. T., J. F. Zhang, W. A. Horne, and R. W. Tsien. 1994. Structural determinants of the blockade of N-type calcium channels by a peptide neurotoxin. *Nature.* 372:272–275.

Fedida, D., R. Bouchard, and F. S. Chen. 1996. Slow gating charge immobilization in the human potassium channel Kv1.5 and its prevention by 4-aminopyridine. *J. Physiol. (Lond.).* 494:377–387.

Feldman, D. H., B. M. Olivera, and D. Yoshikami. 1987. *Omega conus geographus* toxin: a peptide toxin that blocks calcium channels. *FEBS Lett.* 214:295–300.

Fernandez, J. M., F. Bezanilla, and R. E. Taylor. 1982. Distribution and kinetics of membrane dielectric polarization. II. Frequency domain studies of gating currents. *J. Gen. Physiol.* 79:41–67.

Ferreira, G., J. X. Yi, E. Rios, and R. Shirokov. 1997. Ion-dependent inactivation of barium current through L-type calcium channels. *J. Gen. Physiol.* 109:449–461.

Forsythe, I. D., T. Tsujimoto, M. Barnes-Davies, M. F. Cuttle, and T. Takahashi. 1998. Inactivation of presynaptic calcium channel contrib-

utes to synaptic depression at a fast central synapse. *Neuron.* 20: 797–807.

Fox, A. P. 1981. Voltage-dependent inactivation of a calcium channel. *Proc. Natl. Acad. Sci. USA.* 78:953–956.

Grassi, F., and H. D. Lux. 1989. Voltage-dependent GABA-induced modulation of calcium currents in chick sensory neurons. *Neurosci. Lett.* 105:113–119.

Gutnick, M. J., H. D. Lux, D. Swandulla, and H. Zucker. 1989. Voltage-dependent and calcium-dependent inactivation of calcium channel current in identified snail neurones. *J. Physiol. (Lond.).* 412:197–220.

Hadley, R. W., and W. J. Lederer. 1991a. Properties of L-type calcium channel gating current in isolated guinea pig ventricular myocytes. *J. Gen. Physiol.* 98:265–285.

Hadley, R. W., and W. J. Lederer. 1991b. Ca^{2+} and voltage inactivate Ca^{2+} channels in guinea-pig ventricular myocytes through independent mechanisms. *J. Physiol. (Lond.).* 444:257–268.

Hering, S., S. Aczel, M. Grabner, F. Doring, S. Berjukow, J. Mitterdorfer, M. J. Sinnegger, J. Striessnig, V. E. Degtiar, Z. Wang, and H. Glossmann. 1996. Transfer of high sensitivity for benzothiazepines from L-type to class A (BI) calcium channels. *J. Biol. Chem.* 271: 24471–24475.

Hille, B. 1992. Ionic Channels of Excitable Membranes. Sinauer Associates, Sunderland, MA.

Hodgkin, A. L., and A. F. Huxley. 1952. A quantitative description of membrane current and its application to conduction and excitation in nerve. *J. Physiol. (Lond.).* 117:500–544.

Hoshi, T., W. N. Zagotta, and R. W. Aldrich. 1990. Biophysical and molecular mechanisms of *Shaker* potassium channel inactivation. *Science.* 250:533–538.

Hoshi, T., W. N. Zagotta, and R. W. Aldrich. 1991. Two types of inactivation in *Shaker* K^+ channels: effects of alterations in the carboxy-terminal region. *Neuron.* 7:547–556.

Ikeda, S. R. 1991. Double-pulse calcium channel current facilitation in adult rat sympathetic neurones. *J. Physiol. (Lond.).* 439:181–214.

Jones, L. P., P. G. Patil, T. P. Snutch, and D. T. Yue. 1997. G-protein modulation of N-type calcium channel gating current in human embryonic kidney cells (HEK 293). *J. Physiol. (Lond.).* 498:601–610.

Jones, L. P., S-K. Wei, and D. T. Yue. 1998. Mechanism of auxiliary-subunit modulation of neuronal α_{1E} calcium channels. *J. Gen. Physiol.* 112:125–143.

Jones, S. W., and T. N. Marks. 1989. Calcium currents in bullfrog sympathetic neurons. II. Inactivation. *J. Gen. Physiol.* 94:169–182.

Kamp, T. J., M. T. Perez-Garcia, and E. Marban. 1996. Enhancement of ionic current and charge movement by coexpression of calcium channel beta 1A subunit with alpha 1C subunit in a human embryonic kidney cell line. *J. Physiol. (Lond.).* 492:89–96.

Kasai, H., and T. Aosaki. 1988. Divalent cation dependent inactivation of the high-voltage-activated Ca-current in chick sensory neurons. *Pflügers Arch.* 411:695–697.

Klemic, K. G., C. Shieh, G. E. Kirsch, and S. W. Jones. 1998. Inactivation of Kv2.1 potassium channels. *Biophys. J.* 74:1779–1789.

Kuo, C. C., and B. P. Bean. 1994. Na^+ channels must deactivate to recover from inactivation. *Neuron.* 12:819–829.

Lansman, J. B., P. Hess, and R. W. Tsien. 1986. Blockade of current through single calcium channels by Cd^{2+}, Mg^{2+}, and Ca^{2+}. Voltage and concentration dependence of calcium entry into the pore. *J. Gen. Physiol.* 88:321–347.

Liu, Y., M. E. Jurman, and G. Yellen. 1996. Dynamic rearrangement of the outer mouth of a K^+ channel during gating. *Neuron.* 16:859–867.

Lopez-Barneo, J., T. Hoshi, S. H. Heinemann, and R. W. Aldrich. 1993. Effects of external cations and mutations in the pore region on C-type inactivation of *Shaker* potassium channels. *Receptors Channels.* 1:61–71.

McCleskey, E. W., A. P. Fox, D. H. Feldman, L. J. Cruz, B. M. Olivera, R. W. Tsien, and D. Yoshikami. 1987. Omega-conotoxin: direct and persistent blockade of specific types of calcium channels in neurons but not muscle. *Proc. Natl. Acad. Sci. USA.* 84:4327–4331.

McNaughton, N. C. L. and A. D. Randall. 1997. Electrophysiological properties of the human N-type Ca^{2+} channel. 1. Channel gating in Ca^{2+}, Ba^{2+} and Sr^{2+} containing solutions. *Neuropharmacology.* 36: 895–915.

Morad, M., N. W. Davies, J. H. Kaplan, and H. D. Lux. 1988. Inactivation and block of calcium channels by photo-released Ca^{2+} in dorsal root ganglion neurons. *Science.* 241:842–844.

Noceti, F., P. Baldelli, X. Wei, N. Qin, L. Toro, L. Birnbaumer, and E. Stefani. 1996. Effective gating charges per channel in voltage-dependent K^+ and Ca^{2+} channels. *J. Gen. Physiol.* 108:143–155.

Nonner, W. 1980. Relations between the inactivation of sodium channels and the immobilization of gating charge in frog myelinated nerve. *J. Physiol. (Lond.).* 299:573–603.

Olcese, R., R. Latorre, L. Toro, F. Bezanilla, and E. Stefani. 1997. Correlation between charge movement and ionic current during slow inactivation in *Shaker* K^+ channels. *J. Gen. Physiol.* 110:579–589.

Olivera, B. M., G. P. Miljanich, J. Ramachandran, and M. E. Adams. 1994. Calcium channel diversity and neurotransmitter release: the omega-conotoxins and omega-agatoxins. *Annu. Rev. Biochem.* 63:823–867.

Patil, P., D. L. Brody, and D. T. Yue. 1997. Inactivation and G-protein modulation of neuronal voltage-gated calcium channels and short-term plasticity (abstract). *Soc. Neurosci. Abstr.* 23:1193.

Patil, P., D. L. Brody, and D. T. Yue. 1998. Preferential closed-state inactivation of neuronal calcium channels. *Neuron.* 20:1027–1038.

Patil, P. G., M. de Leon, R. R. Reed, S. Dubel, T. P. Snutch, and D. T. Yue. 1996. Elementary events underlying voltage-dependent G-protein inhibition of N-type calcium channels. *Biophys. J.* 71:2509–2521.

Perez-Reyes, E., A. Castellano, H. S. Kim, P. Bertrand, E. Baggstrom, A. E. Lacerda, X. Y. Wei, and L. Birnbaumer. 1992. Cloning and expression of a cardiac/brain beta subunit of the L-type calcium channel. *J. Biol. Chem.* 267:1792–1797.

Pragnell, M., J. Sakamoto, S. D. Jay, and K. P. Campbell. 1991. Cloning and tissue-specific expression of the brain calcium channel beta-subunit. *FEBS Lett.* 291:253–258.

Roux, M. J., R. Olcese, L. Toro, F. Bezanilla, and E. Stefani. 1998. Fast inactivation in *Shaker* K^+ channels: properties of ionic and gating currents. *J. Gen. Physiol.* 111:625–638.

Shirokov, R., R. Levis, N. Shirokova, and E. Rios. 1992. Two classes of gating current from L-type Ca channels in guinea pig ventricular myocytes. *J. Gen. Physiol.* 99:863–895.

Shirokov, R., R. Levis, N. Shirokova, and E. Rios. 1993. Ca(2+)-dependent inactivation of cardiac L-type Ca^{2+} channels does not affect their voltage sensor. *J. Gen. Physiol.* 102:1005–1030.

Sigworth, F. J. 1994. Voltage gating of ion channels. *Q. Rev. Biophys.* 27:1–40.

sigg, D., and F. Bezanilla. 1997. Total charge movement per channel. The relation between gating charge displacement and the voltage sensitivity of activation. *J. Gen. Physiol.* 109:27–39.

Stimers, J. R., F. Bezanilla, and R. E. Taylor. 1985. Sodium channel activation in the squid giant axon. Steady state properties. *J. Gen. Physiol.* 85:65–82.

Stocker, J. W., L. Nadasdi, R. W. Aldrich, and R. W. Tsien. 1997. Preferential interaction of omega-conotoxins with inactivated N-type Ca^{2+} channels. *J. Neurosci.* 17:3002–3013.

Stuhmer, W., F. Conti, M. Stocker, O. Pongs, and S. H. Heinemann. 1991. Gating currents of inactivating and non-inactivating potassium channels expressed in *Xenopus* oocytes. *Pflügers Arch.* 418:423–429.

Stuhmer, W., F. Conti, H. Suzuki, X. D. Wang, M. Noda, N. Yahagi, H. Kubo, and S. Numa. 1989. Structural parts involved in activation and inactivation of the sodium channel. *Nature.* 339:597–603.

Tang, S., A. Yatani, A. Bahinski, Y. Mori, and A. Schwartz. 1993. Molecular localization of regions in the L-type calcium channel critical for dihydropyridine action. *Neuron.* 11:1013–1021.

Tomlinson, W. J., A. Stea, E. Bourinet, P. Charnet, J. Nargeot, and T. P. Snutch. 1993. Functional properties of a neuronal class C L-type calcium channel. *Neuropharmacology.* 32:1117–1126.

Vandenberg, C. A., and F. Bezanilla. 1991. Single-channel, macroscopic, and gating currents from sodium channels in the squid giant axon. *Biophys. J.* 60:1499–1510.

Vassilev, P. M., T. Scheuer, and W. A. Catterall. 1988. Identification of an intracellular peptide segment involved in sodium channel inactivation. *Science.* 241:1658–1661.

Wang, S-Y., and G. K. Wang. 1997. A mutation in segment I-S6 alters slow inactivation of sodium channels. *Biophys. J.* 72:1633–1640.

Werz, M. A., K. S. Elmslie, and S. W. Jones. 1993. Phosphorylation enhances inactivation of N-type calcium channel current in bullfrog sympathetic neurons. *Pflügers Arch.* 424:538–545.

West, J. W., D. E. Patton, T. Scheuer, Y. Wang, A. L. Goldin, and W. A. Catterall. 1992. A cluster of hydrophobic amino acid residues required for fast Na^+-channel inactivation. *Proc. Natl. Acad. Sci. USA.* 89: 10910–10914.

Williams, M. E., P. F. Brust, D. H. Feldman, S. Patthi, S. Simerson, A. Maroufi, A. F. McCue, G. Velicelebi, S. B. Ellis, and M. M. Harpold. 1992. Structure and functional expression of an omega-conotoxin-sensitive human N-type calcium channel. *Science.* 257:389–395.

Yan, Y., Y. Yang, and F. J. Sigworth. 1996. How does W434F block *Shaker* channel current? *Biophys. J.* 70:A190.

Yellen, G., D. Sodickson, T. Y. Chen, and M. E. Jurman. 1994. An engineered cysteine in the external mouth of a K^+ channel allows inactivation to be modulated by metal binding. *Biophys. J.* 66:1068–1075.

Zagotta, W. N., and R. W. Aldrich. 1990. Voltage-dependent gating of Shaker A-type potassium channels in *Drosophila* muscle. *J. Gen. Physiol.* 95:29–60.

Zagotta, W. N., T. Hoshi, and R. W. Aldrich. 1989. Gating of single *Shaker* potassium channels in *Drosophila* muscle and in *Xenopus* oocytes injected with *Shaker* mRNA. *Proc. Natl. Acad. Sci. USA.* 86:7243–7247.

Zagotta, W. N., T. Hoshi, and R. W. Aldrich. 1990. Restoration of inactivation in mutants of *Shaker* potassium channels by a peptide derived from ShB. *Science.* 250:568–571.

Zhang, J. F., P. T. Ellinor, R. W. Aldrich, and R. W. Tsien. 1994. Molecular determinants of voltage-dependent inactivation in calcium channels. *Nature.* 372:97–100.